

# Numerical Heat Transfer, Part A: Applications

## An International Journal of Computation and Methodology

ISSN: 1040-7782 (Print) 1521-0634 (Online) Journal homepage: <http://www.tandfonline.com/loi/unht20>

## Numerical investigation of the pool film boiling of water and R134a over a horizontal surface at near-critical conditions

B. M. Ninge Gowda & B. Premachandran

To cite this article: B. M. Ninge Gowda & B. Premachandran (2017) Numerical investigation of the pool film boiling of water and R134a over a horizontal surface at near-critical conditions, Numerical Heat Transfer, Part A: Applications, 71:1, 44-71, DOI: [10.1080/10407782.2016.1243930](https://doi.org/10.1080/10407782.2016.1243930)

To link to this article: <https://doi.org/10.1080/10407782.2016.1243930>



Published online: 05 Jan 2017.



Submit your article to this journal [↗](#)



Article views: 140



View Crossmark data [↗](#)



Citing articles: 2 View citing articles [↗](#)

# Numerical investigation of the pool film boiling of water and R134a over a horizontal surface at near-critical conditions

B. M. Ningegowda and B. Premachandran

Department of Mechanical Engineering, Indian Institute of Technology Delhi, Hauz Khas, New Delhi, India

## ABSTRACT

Saturated pool film boiling over a flat horizontal surface is investigated numerically for water and refrigerant R134a at near-critical conditions for wall superheats ( $\Delta T_{Sup}$ ) of 2 K, 5 K, 8 K, 10 K, 15 K, and 20 K. The flow is considered to be laminar and incompressible. The governing equations are solved using a finite volume method with a collocated grid arrangement. For capturing the interface in two-phase boiling flows, a Coupled Level Set and Volume of Fluid (CLSVOF) with a multidirectional advection algorithm is used. Both single-mode and multimode boiling models are used for the numerical investigation to understand the effect of computational domain sizes on flow and heat transfer characteristics. In the case of water, the evolution of interface morphology shows the formation of a discrete periodic bubble release cycle occurring at lower Jacob numbers,  $Ja_v \leq 10.2$  ( $\Delta T_{Sup} \leq 8$  K), and the generation of jets of stable vapor film columns occurs at higher  $Ja_v \geq 12.7$  ( $\Delta T_{Sup} \geq 10$  K). In the case of R134a, for all the  $Ja_v$  values considered in this study ( $0.163 \leq Ja_v \leq 1.63$ ), the formation of a discrete periodic bubble release is observed. The results show that multimode boiling model should be used to understand the flow characteristics better. The magnitude of average Nusselt number obtained from the multimode film boiling model is lower than that of the single-mode film boiling model. The Nusselt numbers obtained from the present numerical studies are also compared with the available semiempirical correlations.

## ARTICLE HISTORY


Received 12 April 2016

Accepted 2 September 2016

## 1. Introduction

Boiling heat transfer is encountered in many applications such as heat exchangers, cryogenic equipment, atomic power plants, spacecrafts, and electronics cooling. Although nucleate boiling is preferred, film boiling is unavoidable in many applications. Accurate prediction of film boiling heat transfer is important for designing many thermal systems.

Heat transfer during film boiling over a large horizontal surface is dictated mainly by the vapor release mechanism. Chang [1] was probably the first to relate the instability between the vapor layer and the liquid in film boiling with the Taylor instability and suggested that the wavelength should remain constant and equal to the critical wavelength. Subsequently, he proposed a film boiling model for horizontal surfaces in [2]. Berenson [3] developed a semiempirical model for film boiling over a flat horizontal surface to obtain a heat transfer. He assumed that bubble formation occurs in a square pattern and located at a distance of the most dangerous wavelength of two-dimensional Taylor instability,  $\lambda_{d2}$ , and the bubbles were interconnected with a vapor layer of finite thickness. In his model, one vapor bubble is generated within the area of  $0.5 \lambda_{d2}^2$  and the average height of the bubble above the vapor layer is related to the diameter of the vapor bubble through the relationship provided by

**CONTACT** B. Premachandran  [prem@mech.iitd.ac.in](mailto:prem@mech.iitd.ac.in)  Department of Mechanical Engineering, Indian Institute of Technology Delhi, Hauz Khas, New Delhi 110016, India.

Color versions of one or more of the figures in the article can be found online at [www.tandfonline.com/unht](http://www.tandfonline.com/unht).

© 2017 Taylor & Francis

## Nomenclature

$C_{p,v}$	specific heat of vapor at constant pressure, J/kg · K	$\alpha$	thermal diffusivity, m <sup>2</sup> /s
$g$	acceleration due to gravity, m/s <sup>2</sup>	$\delta(x)$	thickness of the vapor film, m
$h_{lv}$	latent heat of vaporization, J/kg	$\kappa$	mean curvature of the interface, 1/m
$H(\phi)$	smoothed Heaviside function	$\lambda_c$	critical wavelength, $\lambda_c = 2\pi\lambda_o$ , m
$k_f$	thermal conductivity of fluid, W/m · K	$\lambda_{d2}$	two-dimensional most dangerous wavelength, $\lambda_{d2} = \sqrt{3}\lambda_c$ , m
$\vec{n}$	unit normal vector of the interface	$\lambda_o$	capillary length scale, $\lambda_o = \sqrt{[\sigma/\{g(\rho_l - \rho_v)\}]}$ , m
$P$	pressure, Pa	$\mu_f$	dynamic viscosity of the fluid, N · s/m <sup>2</sup>
$S_l$	surface area of the interface line segment, m <sup>2</sup>	$\phi$	level set distance function, m
$S_c$	surface of line segment bounded by the control volume cell, m <sup>3</sup>	$\rho_f$	density of fluid, kg/m <sup>3</sup>
$t_o$	time scale, $t_o = \sqrt{(\lambda_o/g)}$ , s	$\sigma$	surface tension coefficient, N/m
$t_{max}$	maximum time, s	$\tau$	nondimensional time, $(t/t_o)$
$T$	temperature, K	$\Delta T_{Sup}$	wall superheat, $(T_w - T_{Sat})$
$u_o$	velocity scale, $u_o = (\lambda_o/t_o)$ , m/s	<b>Subscripts</b>	
$V_l$	interfacial velocity, m/s	$f$	fluid phase
$\vec{X}$	position vector of the interface	$l$	liquid
<b>Nondimensional parameters</b>		$I$	liquid-vapor interface
$Ja_v$	Jacob number, $C_{p,v}\Delta T_{Sup}/h_{lv}$	$v$	vapor phase
$Gr_v$	Grashof number, $g\lambda_o^3\rho_v(\rho_l - \rho_v)/\mu_v^2$	<b>Superscripts</b>	
$Nu$	Nusselt number	$n$	previous time level
$Pr_v$	Prandtl number, $C_{p,v}\mu_v/k_v$	$n + 1$	current time level

Borishansky [4]. Berenson [3] presented the following correlation for the averaged Nusselt number:

$$Nu_B = 0.425 \left( \frac{Gr_v Pr_v}{Ja_v} \right)^{\frac{1}{4}} \quad (1)$$

Hosler and Westwater [5] carried out boiling experiments with water and Freon-11 and compared their heat transfer coefficient obtained for the film boiling regime for a range of wall superheats ( $\Delta T_{Sup}$ ) with the values obtained from the correlations of Chang [2], Berenson [3], and Borishansky [4]. They commented that the correlation of Berenson [3] predicts heat transfer better compared with the correlations of Chang [2] and Borishansky [4]. They found that the Nusselt number obtained with the model of Chang [2] can be used only as a first cut approximation. From their experimental study, Hosler and Westwater [5] mentioned that the average spacing between bubbles is larger than the critical wavelength,  $\lambda_c$ , but close to the most dangerous Taylor wavelength,  $\lambda_{d2}$ .

Klimenko [6] presented correlations for the average Nusselt number for both laminar and turbulent film boiling over flat horizontal surfaces based on the Reynolds analogy assuming the same cell pattern considered by Berenson [3]. For laminar flow with Grashof number,  $Gr_v \leq 4.03 \times 10^5$ , the Nusselt number correlation was given by Klimenko [6] as follows:

$$Nu_K = 0.19 f_1 (Gr_v Pr_v)^{\frac{1}{3}}$$

where

$$f_1 = \begin{cases} 1 & \text{if } Ja_v > 0.71 \\ 0.89 Ja_v^{-\frac{1}{3}} & \text{if } Ja_v \leq 0.71 \end{cases} \quad (2)$$

Klimenko showed that the relationships provided for the average Nusselt number for both laminar and turbulent film boiling correlate with the experimental data within  $\pm 25\%$  for a wide range of fluids including water and cryogenic liquids. Klimenko and Shelepen [7] used their experimental data of film boiling of helium and argon for further verification of the correlation of Klimenko [6]. The Nusselt number correlations of Berenson [3] and Klimenko [6] are widely used for the heat transfer calculation of film boiling over horizontal flat surfaces even though there are many assumptions. One

of the major assumptions is that the vapor bubbles are released in a square pattern. Even though such a vapor bubble release pattern was observed in the experimental study of Duignan et al. [8], the experimental study of Hosler and Westwater [5] showed that the vapor bubbles were released at random locations.

Rapid advances in the computational methods of two-phase flows in the 1990s enabled researchers to develop numerical models for boiling flows, which could track the interface between the vapor and the liquid. Son and Dhir [9] used a moving mesh method to simulate film boiling of water, benzene, and R113 with an axisymmetric model considering a domain size of  $\sqrt{2/\pi}\lambda_{d2}$  in the radial direction to account for the interface dynamics of both node and antinode. They could capture the bubble growth until the bubble was about to break off from the vapor layer. They pointed out that for the conditions considered in their studies, the Nusselt number obtained from the correlation given by Klimenko is 32% higher than that of Berenson's correlation and their numerical Nusselt number value is 34% lower than the correlation provided by Berenson [3].

As the moving mesh approach cannot capture the vapor bubble departure from the vapor layer in film boiling, Son and Dhir [10] used an Eulerian fixed grid-based level set (LS) method for simulating film boiling of water at near-critical pressures (at 216 and 217 atm.). In their study, they used an axisymmetric model with a computation domain that could capture the bubble growth and departure from a node and an antinode. They investigated the effect of  $\Delta T_{Sup}$  on fluid flow and heat transfer characteristics. At  $\Delta T_{Sup}$  of 10°C, discrete bubbles are released from a node and an antinode alternatively. As  $\Delta T_{Sup}$  increases to 22°C, a stable vapor column forms at the node and periodic bubble release at the antinode was observed. However, at  $\Delta T_{Sup}$  of 30°C, stable vapor column jets formed at both node and antinode. Both the space and the time averaged Nusselt number obtained from their numerical simulations are bound by those predicted from the correlations of [3] and [6]. Based on the results obtained from their numerical simulations carried out for water at 219 atm., they provided the heat transfer correlation for the multimode film boiling model as

$$Nu_{SD} = 0.265(Gr_v Pr_v)^{\frac{1}{4}} \left( Ja_v^{-1} + 0.5 + 1.3 Ja_v^{1/4} \right)^{\frac{1}{4}} \quad (3)$$

Juric and Tryggvason [11] used a front-tracking method to simulate film boiling. With their two-dimensional numerical model, they could capture bubble breakoff from a vapor layer. Welch and Wilson [12] modified the volume of fluid (VOF) method to simulate phase change problems including film boiling. For their film boiling model, the computational domain size of  $\lambda_{d2}/2 \times 3\lambda_{d2}/2$  was used to capture a bubble generation (single-mode model) and release from a thin vapor layer over a heated surface. They also simulated film boiling with the computational domain size of  $\lambda_{d2}/2 \times 3\lambda_{d2}$  for  $\Delta T_{Sup}$  of 5 K and found that the quasi-static behavior of film boiling does not change with the location of outflow boundary conditions. Welch and Rachidi [13] extended the work of [12] on film boiling to investigate the effect of conduction in the heated wall on the flow and heat transfer characteristics. Shin and Juric [14] developed a three-dimensional flow solver with simplified interface tracking and reconstruction algorithms. They evaluated various standard two-phase flow test cases including film boiling. Agarwal et al. [15] carried out a detailed investigation on film boiling of water at near-critical conditions using the VOF method with a computational domain size of  $\lambda_{d2}/2 \times \lambda_{d2}$ .

Esmaeeli and Tryggvason [16] developed a front-tracking/finite difference technique for two-phase flows using both two- and three-dimensional geometries similar to the model of Juric and Tryggvason [11]. They simulated film boiling over a flat surface and compared their results with those of Welch and Wilson [12]. Esmaeeli and Tryggvason [17] carried out numerical simulations of film boiling over a large surface, which captures multiple bubble formations and release from the vapor layer (multi-mode boiling model) with their two-phase flow model presented in [16] for saturated water at 169 bar. As the three-dimensional model is computationally very expensive, they carried out detailed numerical investigations with two-dimensional computational geometries excluding one simulation, all of which were carried out in 3D. They investigated the effect of computational domain by varying the width from  $\lambda_{d2}$  to  $20\lambda_{d2}$  and found that the computational domain size does not affect much the

average Nusselt number obtained at quasi-steady-state conditions. However, they reported that the period and the amplitude of the local Nusselt number variation are irregular due to irregularity in the bubble release cycle. They also investigated the effect of  $\Delta T_{Sup}$  on flow characteristics. It was found that as  $\Delta T_{Sup}$  increases, the periodic bubble release pattern transforms to the formation of vapor columns. They observed that increase in the Jacob number,  $Ja_v$ , does not affect the average distance between the bubble/vapor columns. However, it was observed that the averaged Nusselt number decreases as the  $Ja_v$  increases.

Tomar et al. [18] investigated film boiling of water at near-critical conditions and R134a at near- and far-critical conditions with a single-mode boiling model using a CLSVOF method for a range of  $\Delta T_{Sup}$  values to investigate the frequency of bubble formation. For water,  $\Delta T_{Sup}$  values of 10 K, 15 K, and 17 K were considered. For R134a,  $\Delta T_{Sup}$  values of 10 K, 30 K, and 80 K were considered. Tomar et al. [19] simulated the saturated film boiling of water over a flat horizontal surface with a multimode boiling model. They observed that an increase in  $Ja_v$  shifts the instable bubble growth from the Rayleigh–Taylor instability to the Taylor–Helmholtz instability. Hens et al. [20] investigated the effect of different  $\Delta T_{Sup}$  values for two-dimensional multimode film boiling flow of water at the near-critical conditions of  $P_{Sat} = 21.9$  MPa and  $T_{Sat} = 646$  K.

A similar single-mode boiling model was also used as a test case to validate the boiling flow numerical models developed by Gibou et al. [21], Gada and Sharma [22], Guo et al. [23], Ningegowda and Premachandran [24], and Tsui et al. [25].

From the literature review, it was found that the single-mode film boiling model is extensively used to understand the flow and heat transfer characteristics. Only limited multimode film boiling studies were carried out by [17, 19, 20], which present the flow and heat transfer characteristics closer to reality. The above-mentioned three numerical studies were also carried out only for water. Although Tomar et al. [18] conducted film boiling of R134a, in their study they used the single-mode boiling flow model and no investigation was carried out with the multimode boiling model, which would provide the details related to film boiling phenomena. The applicability of single-mode modeling is also not clear with respect to  $\Delta T_{Sup}$  for various fluids. Hence, in the present study, both single-mode and multimode boiling models are used to simulate film boiling over horizontal flat heater surfaces for near-critical conditions of water and refrigerant R134a at different  $\Delta T_{Sup}$  conditions,  $\Delta T_{Sup}$ .

## 2. Physical problem statement

In this study, saturated film boiling over a flat horizontal surface is investigated numerically for near-critical conditions of water ( $P_{Sat} = 21.9$  MPa;  $T_{Sat} = 646$  K) and refrigerant R134a ( $P_{Sat} = 3.763$  MPa;  $T_{Sat} = 370.46$  K). The horizontal surface is assumed to be maintained at a constant temperature. The flow is assumed to be unsteady, laminar, and incompressible. Two-dimensional computational models are used to investigate the evolution interface morphology and heat transfer characteristic for the  $\Delta T_{Sup}$  values ranging from 2 K to 20 K. Both the single-mode and multimode boiling models are used to investigate the effect of computational domain on the flow and heat transfer characteristics. Constant thermo-physical properties are considered following the work of [18]. The thermo-physical properties of water and R134a at near-critical conditions are given in Tables 1 and 2, respectively.

**Table 1.** Properties of the liquid water and water vapor at the saturation conditions of  $P_{Sat} = 21.9$  MPa and  $T_{Sat} = 646$  K.

Near-critical water properties ( $P_{Cri} = 0.99$ )	Density, $\rho$ (kg/m <sup>3</sup> )	Viscosity, $\mu \times 10^{-6}$ (Ns/m <sup>2</sup> )	Thermal conductivity, $k_f \times 10^{-3}$ (W/mK)	Specific heat, $Cp_f \times 10^3$ (J/kg K)
Liquid phase	402.4	46.7	545	218
Vapor phase	242.7	32.38	538	352
$\sigma = 0.07 \times 10^{-3}$ N/m; $h_{lv} = 276.4 \times 10^3$ J/kg; $P_{Cri} = 22.09$ MPa; $T_{Cri} = 647.29$ K				
Scaling and dimensionless parameters: $\lambda_o = 0.000211$ m, $t_o = 0.00464$ s, $u_o = 0.0455$ m/s, $\lambda_{d2} = 0.0023$ m, $\lambda_c = 0.001328$ m, $Gr_v = 3,425$ , and $Pr_v = 21.17$ .				

**Table 2.** Properties of the liquid refrigerant R134a and its vapor at the saturation conditions of  $P_{Sat} = 3.763$  MPa and  $T_{Sat} = 370.46$  K.

Near-critical R134a properties ( $P_{Cri} = 0.92$ )	Density, $\rho$ (kg/m <sup>3</sup> )	Viscosity, $\mu \times 10^{-6}$ (Ns/m <sup>2</sup> )	Thermal conductivity, $k_f \times 10^{-3}$ (W/mK)	Specific heat, $C_{p_f} \times 10^3$ (J/kg K)
Liquid phase	730.8	56.72	52	5.128
Vapor phase	301.9	21.71	41.5	4.445
$\sigma = 0.182 \times 10^{-3}$ N/m; $h_{lv} = 54.6 \times 10^3$ J/kg; $P_{Cri} = 4.09$ MPa; $T_{Cri} = 374.25$ K				
Scaling and dimensionless parameters: $\lambda_o = 0.000208$ m, $t_o = 0.004604$ s, $u_o = 0.04517$ m/s, $\lambda_{d2} = 0.002263$ m, $\lambda_c = 0.001307$ m, $Gr_v = 2.425 \times 10^5$ , and $Pr_v = 2.325$ .				

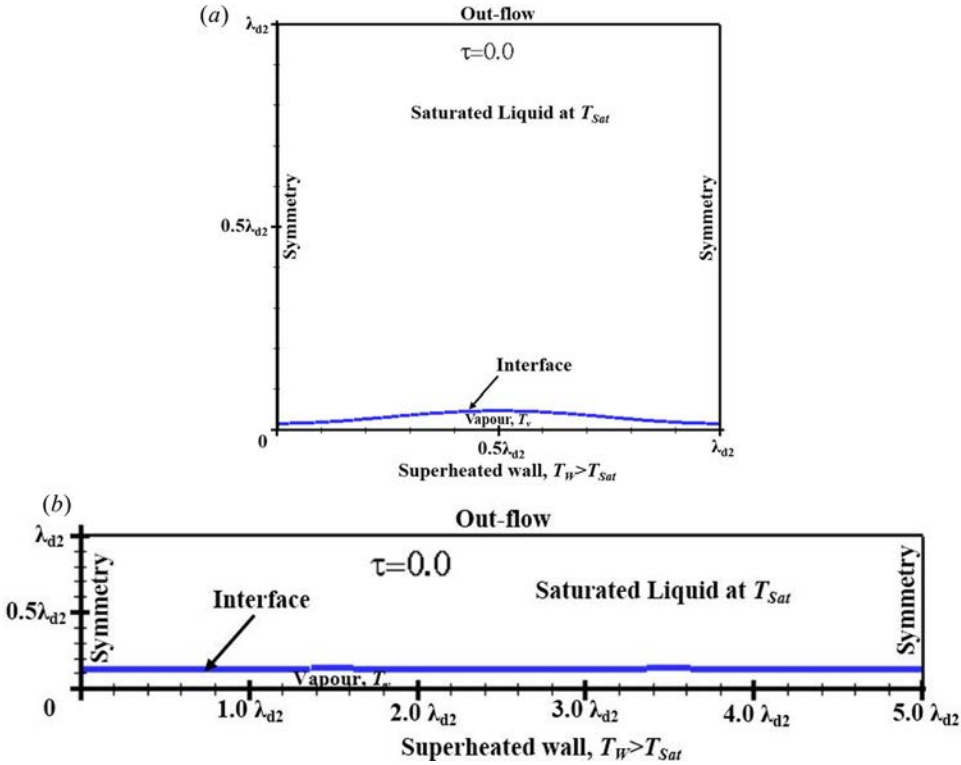
### 3. Numerical modeling

#### 3.1. Computational domains used for single-mode and multimode film boiling models

For simulating saturated film boiling using a two-dimensional single-mode model that could capture the generation of one vapor bubble from a thin vapor layer adjacent to a heated surface, a computational domain size of  $\lambda_{d2} \times \lambda_{d2}$  is considered (in [Figure 1a](#)). In the single-mode film boiling model, the initial unstable thin vapor film thickness,  $\delta(x)$ , is initialized over a superheated wall surface as

$$\delta(x) = \frac{\lambda_{d2}}{64} \left( 4 + \cos\left(\frac{2\pi x}{\lambda_{d2}}\right) \right) \quad (4)$$

For the simulations of multimode saturated film boiling flows that could capture the generation of multiple bubbles from a thin vapor layer adjacent to a heated surface, a computational domain size of  $5\lambda_{d2} \times \lambda_{d2}$  is considered based on the numerical model of Tomar et al. [19] as shown in [Figure 1b](#). Based on Esmaeeli and Tryggvason [17], a randomly perturbed unstable thin vapor film of thickness

**Figure 1.** Computational domain and boundary conditions used for simulating film boiling: (a) single-mode model and (b) multimode model.

$\delta(x)$  is initialized over a large heater surface as

$$\delta(x) = \delta_0 + \frac{\varepsilon}{N} \sum_{i=1}^N r(i) \{ \cos(2\pi ix/L) + \sin(2\pi ix/L) \} \quad (5)$$

In the above expression, uniform film thickness  $\delta_0 = 0.125\lambda_{d2}$ , random wave number  $N = 15$ , wave amplitude of  $\varepsilon = -0.05\lambda_{d2}$ , and  $r(i)$ , which is a randomly generated number ( $0 \leq r(i) \leq 1$ ), are considered.

### 3.2. Governing equations

#### 3.2.1. Single-phase cell region

For the cells in the single-phase region fully filled with either liquid or vapor, the conservation mass, momentum, and energy equations are written as follows:

Continuity equation:

$$\nabla \cdot V = 0 \quad (6)$$

Momentum equation:

$$\rho_f \left( \frac{\partial V}{\partial t} + V \cdot \nabla V \right) = -\nabla P + \nabla \cdot \mu_f [\nabla V + (\nabla V)^T] + \rho_f g \quad (7)$$

In the above equation, the diffusion term  $\nabla \cdot \mu_f [\nabla V + (\nabla V)^T]$  indicates the rate of deformation and the superscript  $T$  indicates the transpose operation.

Energy equation:

$$\rho_f C_{pf} \left( \frac{\partial T}{\partial t} + V \cdot \nabla T \right) = k_f (\nabla^2 T) \quad (8)$$

#### 3.2.2. Interface cell region

For the interface cells where both liquid and vapor phases are present, the continuity Eq. (6) is modified for boiling flows as

$$\int_{S_c} V \cdot \vec{n} ds - \int_{S_I(t)} v_{lv} m_I'' ds = 0 \quad (9)$$

where  $m_I''$  is the interfacial mass flux due to the phase change process, which is computed using the following expression:

$$m_I'' = \|\rho(V - V_I)\| \cdot \vec{n} = \frac{-\|q_I''\| \cdot \vec{n}}{h_{lv}} \quad (10)$$

and  $v_{lv}$  is the inverse of the interfacial density jump condition. It is defined as

$$v_{lv} = \frac{1}{\|\rho\|} = \left( \frac{1}{\rho_l} - \frac{1}{\rho_v} \right) \quad (11)$$

For phase change processes, the second term in Eq. (9) is zero everywhere except at the liquid–vapor interface cell region.  $\|h\|$  is the interfacial enthalpy jump condition and is computed by the latent heat of vaporization as  $h_{lv} = h_v - h_l$  and  $\|q_I''\|$  is the interfacial conduction heat flux jump condition and is computed using Fourier's law of heat conduction.

The momentum Eq. (7) is modified for the interfacial cell to account for the surface tension force as

$$\rho_f \left( \frac{\partial V}{\partial t} + V \cdot \nabla V \right) = -\nabla P + \nabla \cdot \mu_f [\nabla V + (\nabla V)^T] + \rho_f g + F_{st} \quad (12)$$



where  $F_{st}$  is the interfacial surface tension force per unit volume. In this study, the interfacial surface tension force is calculated using the Continuum Surface tension Force (CSF) model of Brackbill et al. [26]. In the CLSVOF method [27, 28], the interfacial surface tension force is computed as  $F_{st} = \sigma \kappa \nabla H(\phi)$ , where  $\sigma$  is the surface tension coefficient and is taken as a constant value,  $\vec{n}$  is the unit normal vector,  $\kappa$  is the mean curvature of the phase interface, and  $H(\phi)$  is the smoothed Heaviside function. In the CLSVOF method, the unit normal vector  $\vec{n}$  and mean curvature  $\kappa$  are accurately computed as compared to the VOF method using the gradients of a smoothed continuous LS function  $\phi$  [28] as follows:

$$\vec{n} = \frac{\nabla \phi}{|\nabla \phi|} \text{ and } \kappa = -\nabla \cdot \left( \frac{\nabla \phi}{|\nabla \phi|} \right) = - \left( \frac{\phi_y^2 \phi_{xx} - 2\phi_x \phi_y \phi_{xy} + \phi_x^2 \phi_{yy}}{(\phi_x^2 + \phi_y^2)^{\frac{3}{2}}} \right)$$

At the liquid-vapor interface cells region, the thermo-physical properties of the fluids are discontinuous and this leads to numerical instability [27]. To avoid numerical instability, in the whole computational domain, the thermo-physical properties are calculated in terms of the smoothed Heaviside function,  $H(\phi)$  [27, 28]. The smoothed Heaviside function,  $H(\phi)$ , in the domain is computed using the continuous LS distance function,  $\phi$ , as

$$H(\phi) = \begin{cases} 1 & \text{LiquidPhase, if } \phi > \varepsilon \\ 0.5 + \left(\frac{\phi}{2\varepsilon}\right) + \frac{1}{2\pi} \sin\left(\frac{\pi\phi}{\varepsilon}\right) & \text{Interface, if } |\phi| \leq \varepsilon \\ 0 & \text{VapourPhase, if } \phi < -\varepsilon \end{cases} \quad (13)$$

where  $\varepsilon$  is the width of the interface region and is computed as 1.5 times the domain grids size  $\Delta x$ , i.e.,  $\varepsilon = 1.5\Delta x$ . In whole domain cells, for any thermo-physical property,  $\gamma$  such as density,  $\rho_f$  dynamic viscosity,  $\mu_f$  specific heat at constant pressure,  $C_{p,f}$  and thermal conductivity,  $k_f$  are calculated based on the smoothed Heaviside function,  $H(\phi)$ , as follows:

$$\gamma_f = \gamma_v + (\gamma_l - \gamma_v)H(\phi) \quad (14)$$

### 3.3. Multidirectional advection algorithms of the CLSVOF interface capturing method

For capturing dynamic liquid-vapor interfaces, a CLSVOF method with a multidimensional advection algorithm proposed by Ningegowda and Premachandran [24] is used. For the multidirectional advection of the VOF function, the method proposed by Lopez et al. [29] and Lopez and Hernandez [30] is used. In the present CLSVOF method, the advection equations of both VOF and LS functions are solved explicitly using fixed Eulerian grids. In the VOF method, the volume fraction  $F$  is geometrically initialized in the domain and its value is  $F = 1$  for the cells filled with liquid,  $F = 0$  for the cell fully filled with vapor, and  $0 < F < 1$  at the interfacial cell region. For simulating boiling flows, the VOF advection equation can be written as

$$\frac{\partial F}{\partial t} + \nabla \cdot (VF) = F_{mt} \quad (15)$$

where  $F_{mt}$  is the rate of the volume fraction generated due to the interfacial phase change process.

The VOF advection Eq. (15) is discretized using the first-order explicit scheme as

$$F^{n+1} = F^n - \frac{1}{V_\Omega} \int_{t_n}^{t_{n+1}} \int_{\Omega} \nabla \cdot (VF) d\Omega dt + F_{mt} \Delta t \Delta \Omega \quad (16)$$

In the present study, the VOF advection fluxes at the cell faces are calculated using the geometric Piecewise Linear Interface Calculation (PLIC) reconstruction algorithm [31, 32].



In the LS method, the LS function  $\phi$  is the shortest distance function computed from the phase interface [33]. The LS function  $\phi$  is zero at the interface ( $\phi = 0$ ), and is a positive distance function in the continuous liquid phase region ( $\phi > 0$ ) and is a negative distance function in the discrete vapor phase region ( $\phi < 0$ ). For boiling flows, the LS advection equation can be written as

$$\frac{\partial \phi}{\partial t} + (V_{mt} \cdot \nabla) \phi = 0 \quad (17)$$

The total velocity at the interface cell region is  $V_{mt} = V_{cell} + V_I \vec{n}$ , where  $V_{cell}$  is the cell centroid velocity components and  $V_I = v_{lg} m_I''$  is the interfacial velocity due to heat and mass transfer across the interface. The multidimensional advection algorithms of the CLSVOF method used in this study have been described in detail by Ningegowda and Premachandran [24]. This method is extensively validated using standard benchmark problems for advection algorithm, interfacial surface tension force, and the phase change models.

### 3.4. Boundary and initial conditions

The boundary conditions used for the single-mode boiling model and the multimode boiling model are the same. These boundary conditions are considered based on [12, 15, 18–20]. At the bottom boundary of the computational domain (at  $y = 0$ ), the no-slip boundary condition is imposed to specify it as a superheated isothermal wall. The boundary conditions are written as

$$u = v = 0, \quad T(x, 0) = T_W = T_{Sat} + \Delta T_{Sup}$$

where  $T_{Sat}$  is the saturation temperature of the fluid and  $\Delta T_{Sup}$  is the wall superheat.

For boundaries at both the left (at  $x = 0$ ) and right (at  $x = L$ ) sides of the computational domain, the symmetric boundary conditions are imposed:

$$u = 0 \text{ and } \frac{\partial v}{\partial x} = \frac{\partial T}{\partial x} = \frac{\partial F}{\partial x} = \frac{\partial \phi}{\partial x} = 0$$

At the top boundary, the following out-flow boundary conditions are used:

$$\text{at } y = H \quad \frac{\partial u}{\partial y} = \frac{\partial v}{\partial y} = \frac{\partial T}{\partial y} = \frac{\partial F}{\partial y} = \frac{\partial \phi}{\partial y} = 0 \text{ and } P = P_{out}$$

where  $P_{out}$  is the saturation pressure less than the hydrostatic pressure difference obtained with respect to the initial liquid–vapor interface.

In the present study, a linear variation of the temperature profile has been initialized inside the superheated vapor phase region. Initially, a zero velocity field is also considered in the whole computational domain.

### 3.5. Numerical solution procedures

In this numerical study, a finite volume method based on a collocated grid approach is used for solving the governing equations numerically. For velocity and pressure coupling, the Semi-Implicit Method for Pressure Linked Equations (SIMPLE) algorithm is used. The unsteady terms are discretized using the first-order accurate explicit scheme. The convective terms of momentum and energy equations are discretized using a third-order accurate Quadratic Upstream Interpolation for Convective Kinematics (QUICK) scheme [34] and the diffusion terms are discretized using a second-order accurate Central Differencing Scheme (CDS) scheme. For interface capturing, the multidirectional advection-based CLSVOF method of [24] is used. The convective terms in the LS advection equation are discretized using the second-order accurate Essentially Non-Oscillatory (ENO) scheme presented in [28]. The redistancing of the LS function is carried using the PLIC (Piecewise Linear Interface Calculation)-VOF-based geometric reconstruction algorithm [27, 28].

### 3.6. Selection of the grid size and time step

In the present grid independence study, the variations of the liquid–vapor interface morphology, the local, and space averaged Nusselt numbers are compared for uniform grid sizes of  $120^2$ ,  $240^2$ ,  $360^2$ , and  $480^2$  for the near-critical conditions of water ( $P_{Sat} = 21.9$  MPa,  $T_{Sat} = 646.15$  K) at  $\Delta T_{Sup}$  of 10 K and the time step of  $\Delta t = 0.01\Delta x$ . In the first periodic bubble release cycle, the grid sizes of  $360^2$  and  $480^2$  show negligible variations in the evolution of the phase interface as compared to the other coarser grids (Figure 2a). The variation of local Nusselt number at the nondimensional time  $\tau = 19.39$  is shown in Figure 2b. The space averaged Nusselt number obtained for grid sizes of  $120^2$ ,  $240^2$ ,  $360^2$ , and  $480^2$  are 2.044, 1.717, 1.61, and 1.593, respectively. As the percentage difference in the average Nusselt number obtained from the grid sizes of  $360^2$  and  $480^2$  is only 1.067%, in the present study, a uniform grids size of  $360^2$  is selected as the optimum grid size for the single-mode boiling flow model for simulating film boiling of water. The same grid size was also used for the simulation of film boiling of R134a.

The time step was selected based on the numerical simulations carried out with the Courant–Friedrichs–Lewy (CFL) numbers,  $C = 0.25, 0.1, 0.025$ , and  $0.01$  for water at  $\Delta T_{Sup}$  of 10 K using a grid size of  $360^2$ . The interface morphology obtained for various CFL numbers at  $\tau = 21.54$  is shown in Figure 2c. For the CFL numbers of  $0.025$  and  $0.01$ , the interface morphology and the variation of

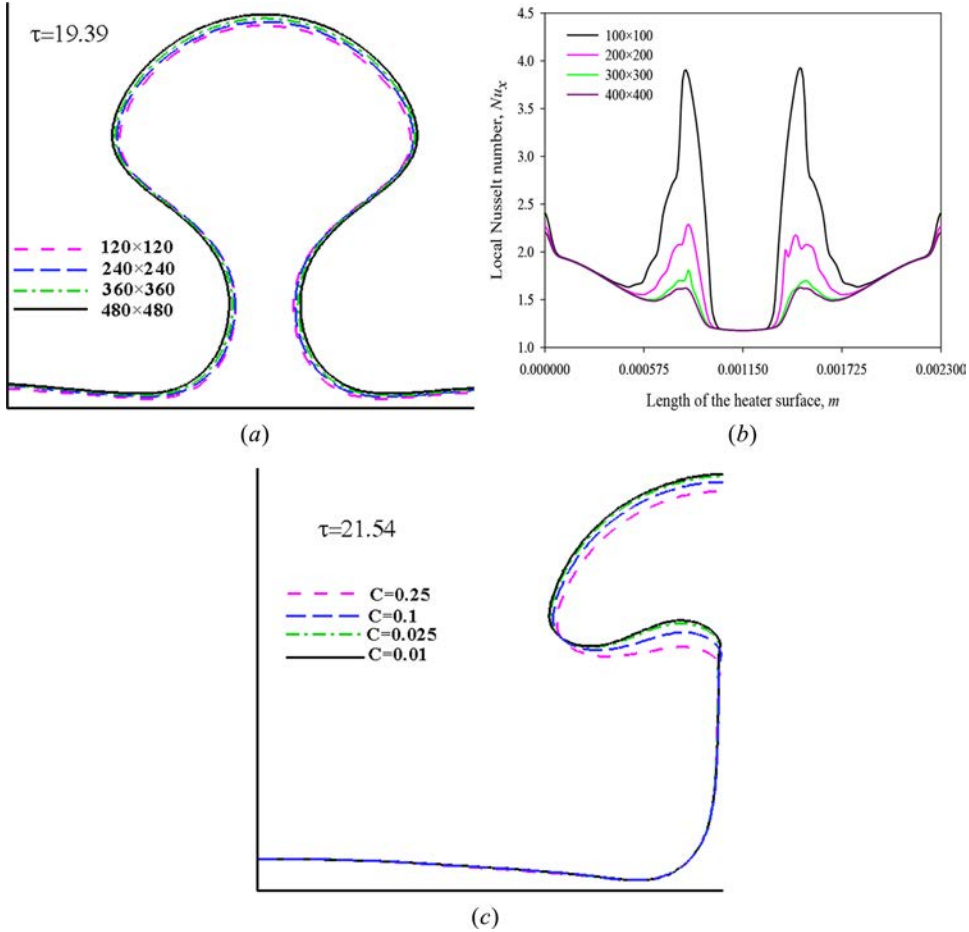


**Figure 2.** Grid independence and time step convergence study of single-mode film boiling of water at near-critical conditions for Jacob number  $Ja_v = 12.74$  ( $\Delta T_{Sup} = 10$  K): (a) the liquid–vapor interface morphology, (b) distribution of the local Nusselt number, and (c) effect of CFL number,  $C$ .

space averaged Nusselt number become insignificant. Hence, in this study, a CFL number  $C$  of 0.01 is selected. For all simulations of the single-mode film boiling model for water and R134a, a uniform grid size of  $360^2$  and the time step size  $\Delta t$  of  $0.01 \Delta x$  were used.

Numerical simulations of multimode boiling, even for the two-dimensional geometry, are computationally very expensive [17]. For the multimode film boiling model, for each  $\lambda_{d2}$ , a uniform grid size of 240 was used by both Tomar et al. [19] and Hens et al. [20] with the CLSVOF method. Esmaeeli and Tryggvason [17] used a uniform grid size of 128 for each  $\lambda_{d2}$  with the front-tracking method. In the present study, for the simulations of multimode saturated film boiling flows using the CLSVOF method, the computational domain size of  $5\lambda_{d2} \times \lambda_{d2}$  is discretizing using a uniform grid size of  $1,200 \times 240$  and time step of  $\Delta t = 0.01 \Delta x$ .

## 4. Results and discussions

Film boiling at near-critical conditions of water ( $P_{Sat} = 21.9$  MPa,  $T_{Sat} = 646.15$  K) and R134a ( $P_{Sat} = 3.763$  MPa,  $T_{Sat} = 370.16$  K) are investigated using both single-mode and multimode boiling models for the  $\Delta T_{Sup}$  values of 2 K, 5 K, 8 K, 10 K, 15 K, and 20 K. For investigating film boiling flows, the scaling parameters are obtained from the thermo-physical properties of the working fluids. The computational domain sizes are computed based on the most dangerous Taylor wavelength,  $\lambda_{d2}$ .

In the present numerical study, the local Nusselt number over the flat surface is computed as

$$Nu_x = \frac{\lambda_o}{(T_W - T_{Sat})} \left. \frac{\partial T}{\partial y} \right|_W \quad (18)$$

where  $\lambda_o$  is the capillary length scale. The space averaged Nusselt number over the horizontal flat surface is calculated as

$$Nu_{L,Avg} = \frac{1}{L} \int_0^L Nu_x dx \quad (19)$$

The time averaged Nusselt number over the horizontal flat surface is written as

$$Nu_{T,Avg} = \frac{1}{t_{max}} \int_0^{t_{max}} Nu_{L,Avg} dt \quad (20)$$

### 4.1. Saturated film boiling of water

#### 4.1.1. Single-mode film boiling flow of water

In this subsection, the results obtained from the numerical simulations carried out for saturated film boiling of water at near-critical conditions with the single-mode model are presented to investigate the effect of  $\Delta T_{Sup}$  on the flow and heat transfer characteristics. Figure 3 shows the evolution of the liquid-vapor interface morphology during the formation of the first ebullition cycle at various  $Ja_v$  ( $\Delta T_{Sup}$ ) conditions. In the present study, up to  $Ja_v \leq 10.19$  ( $\Delta T_{Sup} \leq 8$  K), the periodic bubble formation and departure of discrete vapor bubbles are observed alternatively at the node and the anti-nodes as shown in Figures 3a–c. At higher  $Ja_v$  values of 12.735 and 19.1, the formation of jets of stable vapor columns is observed at both nodes and antinodes as shown in Figures 3d,e. In the present study and in the study of Tomar et al. [18], the size of the computational domain considered is  $\lambda_{d2} \times \lambda_{d2}$ . Hence, it is not possible to visualize the departure of bubbles at the end of the vapor column as it was presented in Son and Dhiri [10], who carried out numerical simulations for the computational domain height more than twice the size considered in the present study. The release of vapor bubbles at the end of the vapor column was also observed by Reimann and Grigull [35] in the experimental studies of film boiling of water over a thin wire at near-critical conditions. The numerical investigation of Welch and Wilson [12] shows that the computational domain size of a single-mode boiling model

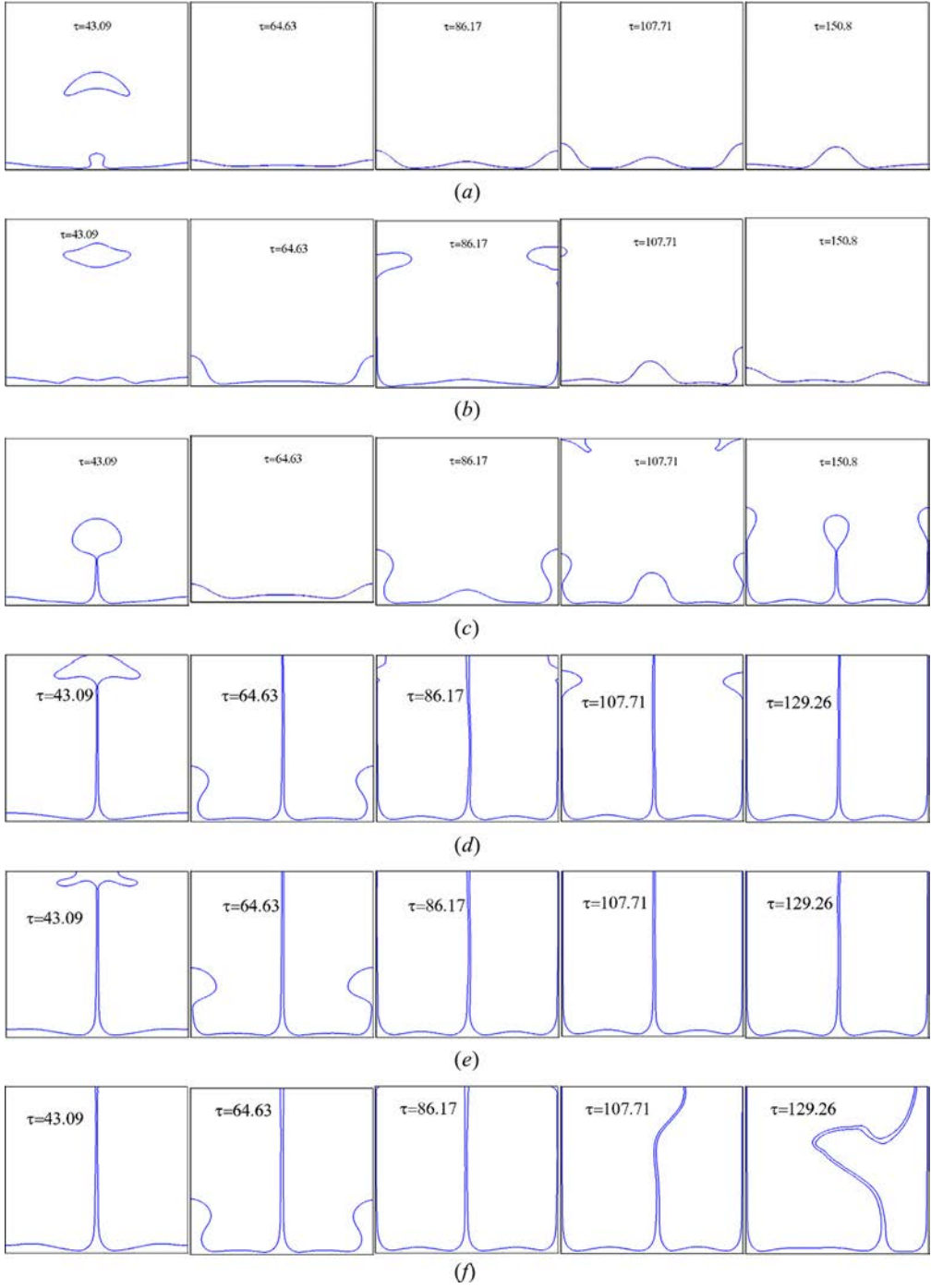


**Figure 3.** Interface morphologies of the periodic bubble release cycle obtained using the single-mode boiling model for water at different Jacob numbers (a)  $Ja_v = 2.55$  ( $\Delta T_{Sup} = 2$  K), (b)  $Ja_v = 6.37$  ( $\Delta T_{Sup} = 5$  K), (c)  $Ja_v = 10.19$  ( $\Delta T_{Sup} = 8$  K), (d)  $Ja_v = 12.735$  ( $\Delta T_{Sup} = 10$  K), (e)  $Ja_v = 19.1$  ( $\Delta T_{Sup} = 15$  K), and (f)  $Ja_v = 25.47$  ( $\Delta T_{Sup} = 20$  K).

along the direction of bubble departure does not affect the statistical behavior of film boiling. For  $Ja_v = 25.47$ , the vapor column becomes unstable at  $\tau \geq 86.17$ . Similar instability of long vapor column was also observed by Gibou et al. [21] for 10 K for a two-phase fluid at  $P_{Sat} = 1.0135 \times 10^5$  Pa and

$T_{Sat} = 500$  K as considered. The flow patterns obtained corresponding to a discrete bubble release cycle at  $Ja_v = 10.19$  (at  $\tau = 47.4$ ) and stable vapor column observed at the node at  $Ja_v = 25.47$  (at  $\tau = 81.86$ ) are shown in [Figures 4a](#) and [b](#), respectively.

The variations of space and time averaged Nusselt number with respect to  $\tau$  obtained for  $Ja_v$  values of 2.547 ( $\Delta T_{Sup} = 2$  K) and 6.367 ( $\Delta T_{Sup} = 5$  K) in the present study are shown in [Figure 5](#). [Figure 5a](#) shows the periodic variation of space averaged Nusselt numbers for five periodic bubble release cycles at  $Ja_v = 2.547$  ( $\Delta T_{Sup} = 2$  K). From these results, it is found that each periodic ebullition cycle occurs approximately for  $\tau \sim 125$ . This figure shows that the average Nusselt number obtained from the semiempirical correlation of Berenson [3] and Klimenko [6] is also presented. This plot shows that the time averaged Nusselt number obtained from the present study is underpredicted compared with the values obtained from the correlations of Berenson [3] and Klimenko [6]. [Figure 5b](#) shows the periodic variation of the space and time averaged Nusselt numbers for water at  $Ja_v = 6.367$  ( $\Delta T_{Sup} = 5$  K). The variation of space averaged Nusselt number shows that a periodic bubble release cycle occurs approximately at  $\tau = 100$ . The duration of one ebullition cycle further decreases as  $\Delta T_{Sup}$  increases to 8 K.

#### 4.1.2. Multimode film boiling of water at near-critical conditions

The periodic evolution of the interface morphology of saturated film boiling at near-critical conditions of water for  $Ja_v = 2.547$  ( $\Delta T_{Sup} = 2$  K) and 6.367 ( $\Delta T_{Sup} = 5$  K) obtained using the multimode film boiling model is shown in [Figure 6](#). For both  $Ja_v$  values, the results show the formation of large-sized vapor bubbles during the first ebullition cycle at the nodes due to the effect of the initial vapor film thickness,  $\delta(x)$ . From the second periodic bubble release cycle onward, for  $\tau \geq 150$ , the average bubble size is almost constant. Within the computational domain, the vapor bubbles are released at nodes and antinodes randomly, excluding at two locations, where two stable vapor columns are formed as shown in [Figure 6a](#). The bubbles are also released periodically at the end (or tip) of the stable vapor columns. The experimental investigation of saturation film boiling of  $\text{CO}_2$  at near-critical condition carried out by Abadzic and Goldstein [36] also shows the release of vapor bubble at the tip of the vapor column at few locations and periodic bubble release at the other locations at 71.4 bar. Although the geometry of the heating surface and fluid considered in the present study are not the same as those of [36], the mechanism of bubble release pattern presented in their photograph and the present numerical results provide better insight into the mechanism of vapor release. The numerical results of Esmaeeli and Tryggvason [17] also show a similar pattern for the case of saturation film boiling of water at 169 bar for  $Ja_v = 0.064$  ( $\Delta T_{Sup} = 3.2$  K). Unlike the multimode boiling model, no

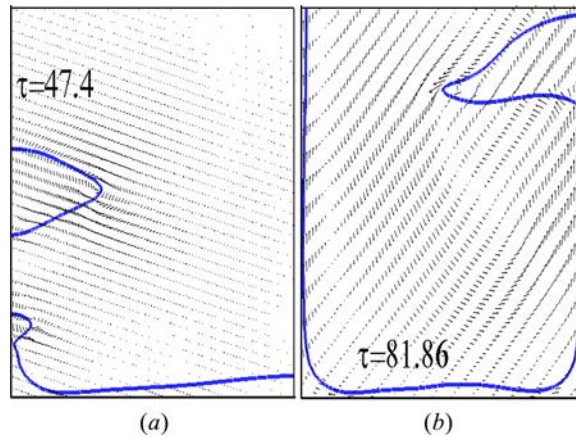


**Figure 4.** The velocity vector plots for the single-mode boiling model for water at near-critical conditions. (a) The formation of discrete bubble at Jacob number,  $Ja_v = 10.19$  and (b) the formation of jets of stable vapor column at Jacob number  $Ja_v = 25.47$ .

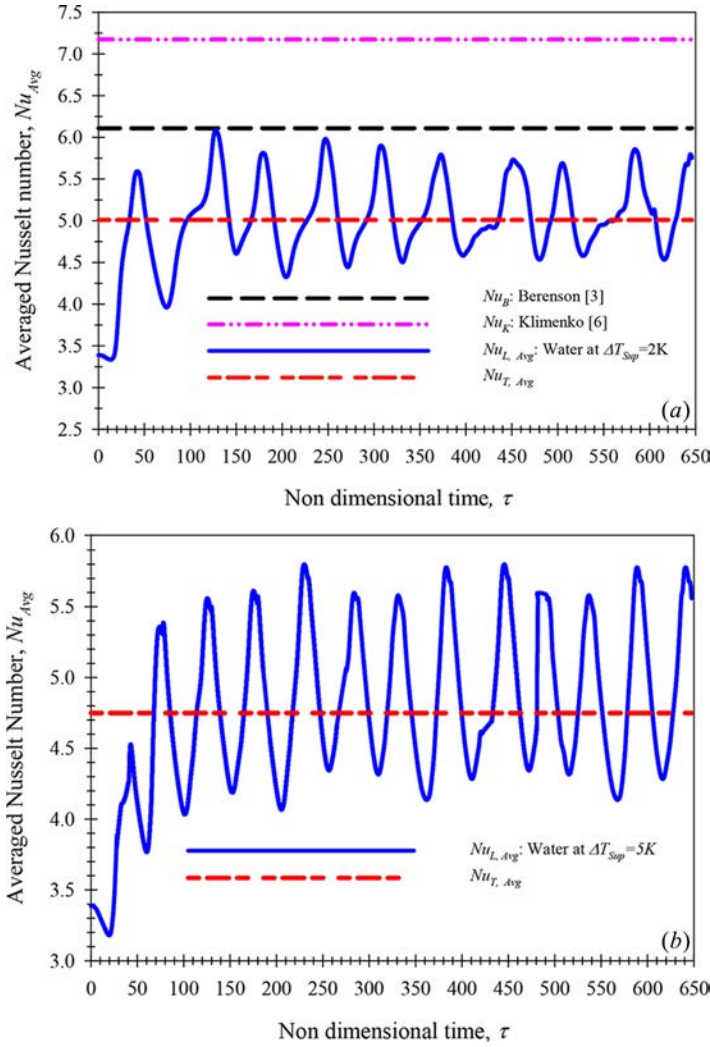


**Figure 5.** Transient variations of the space and the time averaged Nusselt numbers obtained with the single-mode film boiling model for water at different Jacob numbers: (a)  $Ja_v = 2.55$  and (b)  $Ja_v = 6.37$ .

vapor column is formed in the case of the single-mode boiling flow model for both values of  $Ja_v = 2.547$  and  $6.367$  in [Figures 3a](#) and [3b](#), respectively.

At  $Ja_v = 6.367$  ( $\Delta T_{Sup} = 5$  K), the numerical results show the formation of stable vapor columns at two nodes ([Figure 6b](#)). At the remaining nodes and antinodes, the discrete vapor bubbles are released periodically. At this  $Ja_v$ , the length of the vapor columns increases and the bubble release might be at the end of the column, which is beyond the computational domain selected. A similar trend was also observed at  $Ja_v = 12.735$  ( $\Delta T_{Sup} = 10$  K) as well.

[Figure 7](#) shows the evolution of the liquid–vapor interface morphology and the corresponding spatial variations of the local Nusselt numbers at various  $\tau$  values for  $Ja_v = 6.367$ . At any location of bubble formation and growth, the thickness of the vapor layer increases. Hence, the heat transfer rate decreases at this location. After the bubble departure, the remaining vapor draws in toward the wall and the thickness of the vapor layer decreases continuously up to a certain thickness, which is much lower than the average vapor layer. This leads to an increase in the heat transfer rate due to increase in the temperature gradient. Hence, at a location of bubble growth and departure, the heat



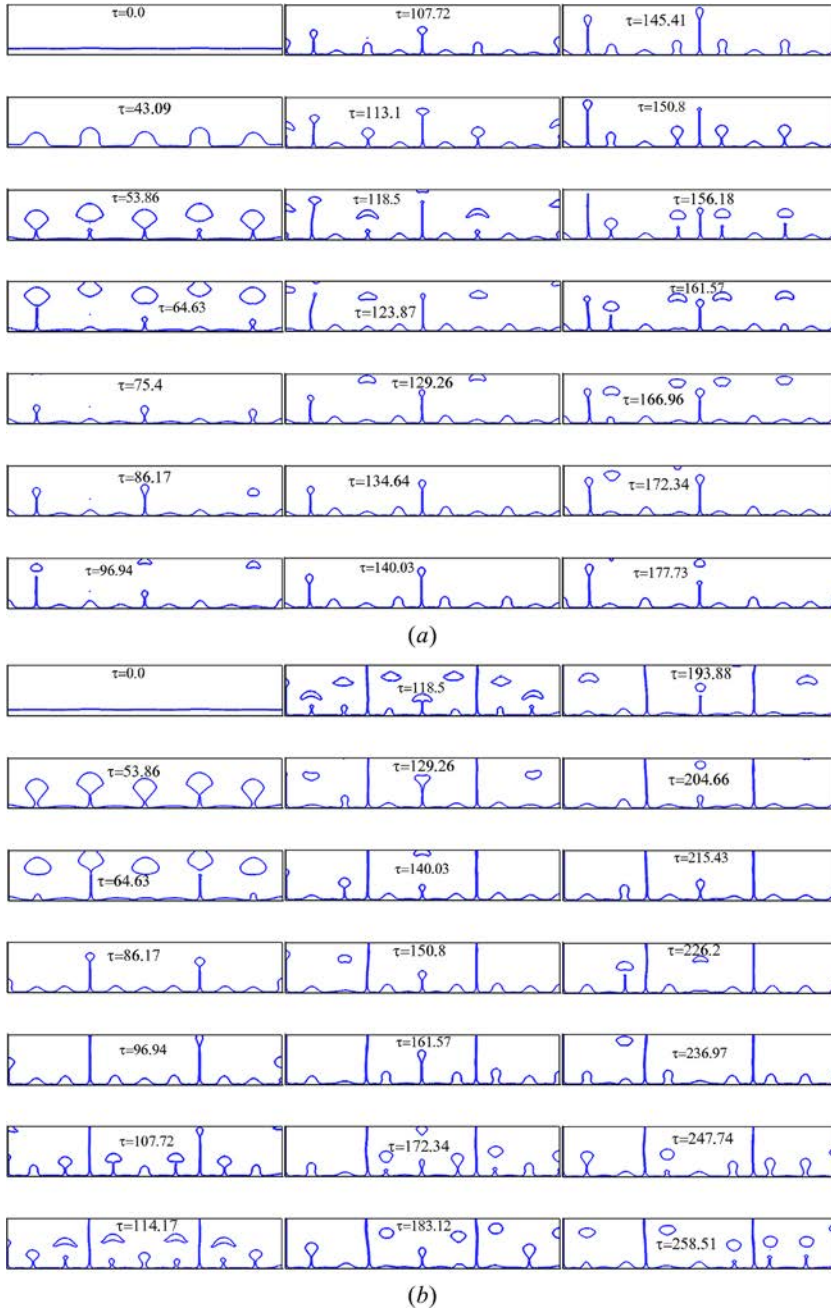


**Figure 6.** Transient evolution of the discrete periodic bubble release cycle obtained with the multimode film boiling model for water at near critical Jacob numbers: (a)  $Ja_v = 2.55$  and (b)  $Ja_v = 6.37$ .

transfer rate at the heated surface decreases during the vapor bubble growth and increases as the vapor layer locally withdraws toward the wall.

Figures 8a and b shows the interface morphology at different  $\tau$  values for  $Ja_v = 19.1$  and 25.47, respectively. At  $Ja_v = 19.1$  (or  $\Delta T_{Sup} = 15$  K), after  $\tau = 118.5$ , stable vapor columns are formed at both nodes and antinodes. A similar trend was also observed in the case of the single-mode boiling model simulations as shown in Figure 3e. The similar pattern of stable water column was also observed in



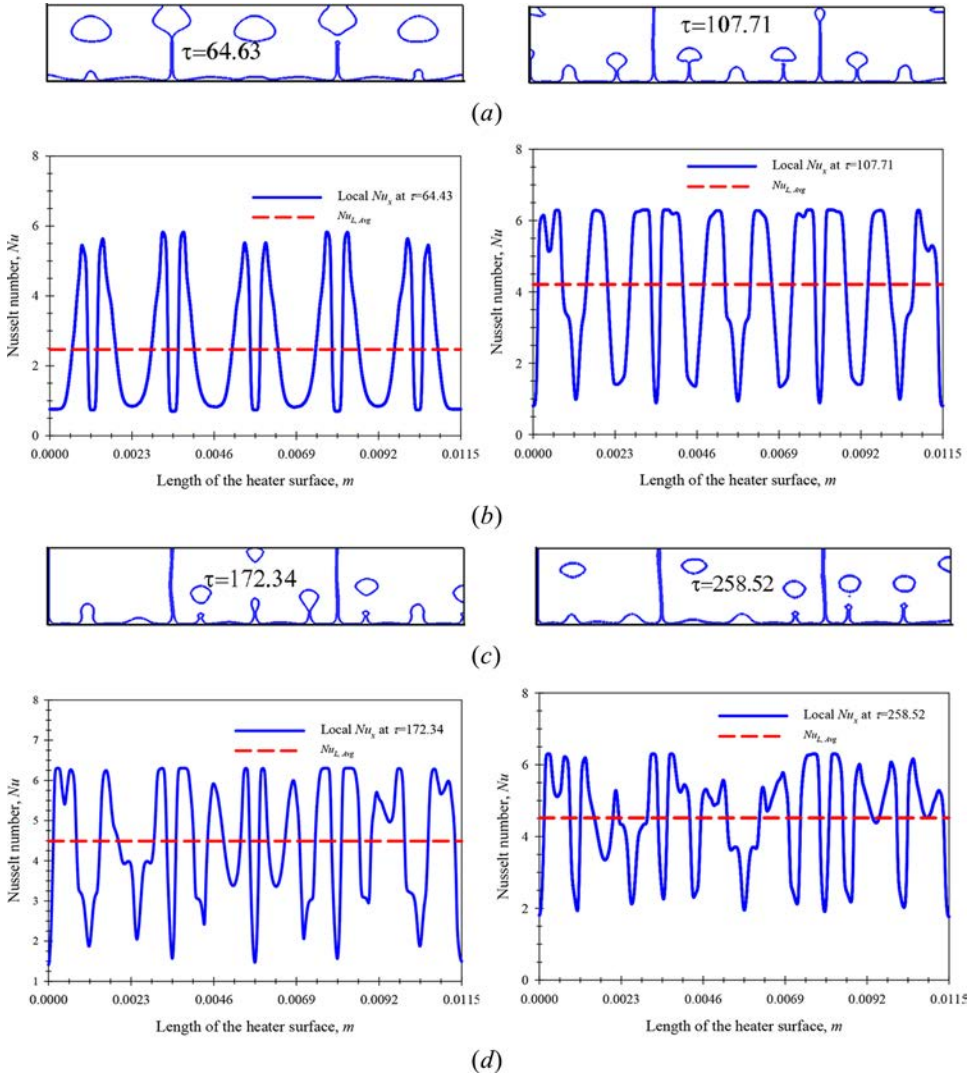


**Figure 7.** Interface evolution obtained from the multimode film boiling model and the corresponding variation of local Nusselt number for water at Jacob number  $Ja_v = 6.37$ : (a) interface morphology obtained at  $\tau = 64.63$  and  $\tau = 107.71$ , (b) the variation of local Nusselt number obtained at  $\tau = 64.63$  and  $\tau = 107.71$ , (c) interface morphology obtained at  $\tau = 172.34$  and  $\tau = 258.52$ , and (d) the variation of local Nusselt number obtained at  $\tau = 172.34$  and  $\tau = 258.52$ .

the experimental study of film boiling over a thin wire at near-critical conditions by Reimann and Grigull [35]. At  $Ja_v = 25.47$ , as shown in Figure 8b, the vapor columns are not stable and vapor bubble formation is noticed at two locations within the computational domain of width,  $L$  is  $5\lambda_{d2}$ .

The trend on the evolution of interface morphology observed in the present study closely agrees with that of Esmaeeli and Tryggvason [17], who investigated saturated film boiling of water at 169 bar and 625 K using a two-dimensional multimode model with the computational domain width of  $10\lambda_{d2}$ . They also observed the release of discrete vapor bubbles at many locations and three stable vapor columns at low  $Ja_v = 0.064$  ( $\Delta T_{Sup} = 3.2$  K), similar to the present numerical study. At medium values of  $Ja_v$  of 0.213 ( $\Delta T_{Sup} = 10.65$  K) and 0.421 ( $\Delta T_{Sup} = 21.35$  K), their results show stable vapor columns without any discrete vapor bubble formation from the vapor film layer. At the higher  $Ja_v$  of 0.853 ( $\Delta T_{Sup} = 42.65$  K), they observed a vapor bubble formation due to the instability of vapor columns similar to what is observed at  $Ja_v = 25.47$  ( $\Delta T_{Sup} = 20$  K) in the present study. Stable vapor columns

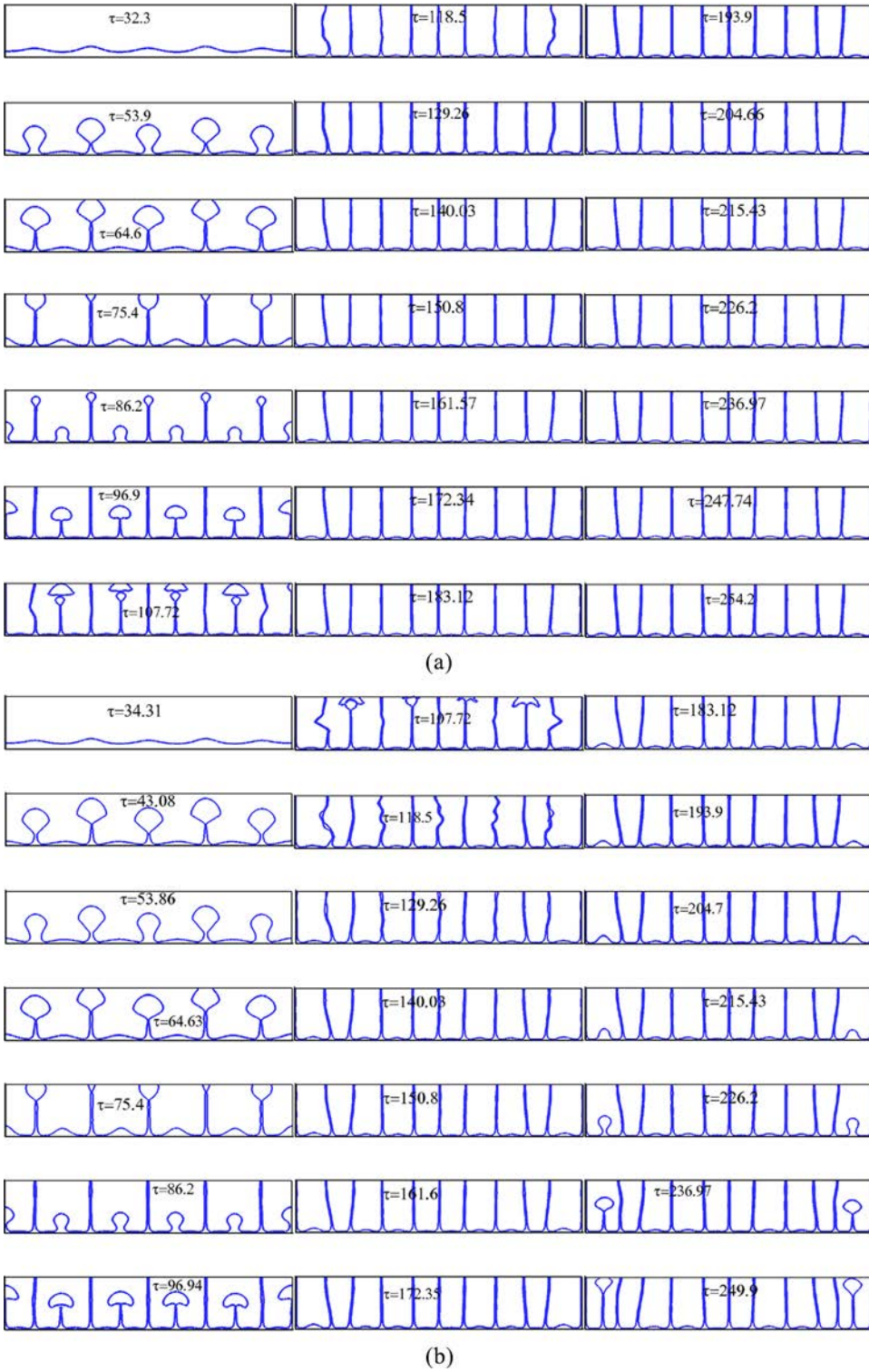


**Figure 8.** Evolution of the interface morphology obtained with the multimode film boiling model for water at different Jacob numbers: (a)  $Ja_v = 19.1$  and (b)  $Ja_v = 25.47$ .

were observed by Son and Dhir [10] for near-critical conditions of water at  $Ja_v = 38.205$  ( $\Delta T_{Sup} = 30$  K) for the same conditions considered in the present numerical study. In their study, they used an axisymmetric model for simulating film boiling over a horizontal flat plate. However, a two-dimensional plane geometry is considered in the present study similar to Tomar et al. [19]. Hence, the  $Ja_v$  at which the formation of vapor columns were observed in the present numerical study and the study of Son and Dhir [10] differs. However, the trend in the flow characteristics observed in the present study and the study of Son and Dhir [10] is similar. Klimenko [6] mentioned that film boiling is laminar if  $Gr_v \leq 4.03 \times 10^5$ . In the present study, the Grashof number  $Gr_v = 3,425$  and the flow characteristics observed at  $Ja_v = 25.47$  ( $\Delta T_{Sup} = 20$  K) also exhibit laminar flow.

Figure 9 shows the distance between the nodes and antinodes at various  $Ja_v$  values in terms of  $\lambda_{d2}$  at ( $\tau = 177.73$ ). The smallest and the largest distance between two consecutive nodes are  $0.87\lambda_{d2}$  and  $1.1\lambda_{d2}$ , respectively. The average spacing between the nodes obtained for the  $Ja_v$  values of 2.547, 6.367, 19.103, and 25.47 are  $1.02\lambda_{d2}$ ,  $0.9925\lambda_{d2}$ ,  $0.97\lambda_{d2}$ , and  $0.93\lambda_{d2}$ , respectively. Holser and

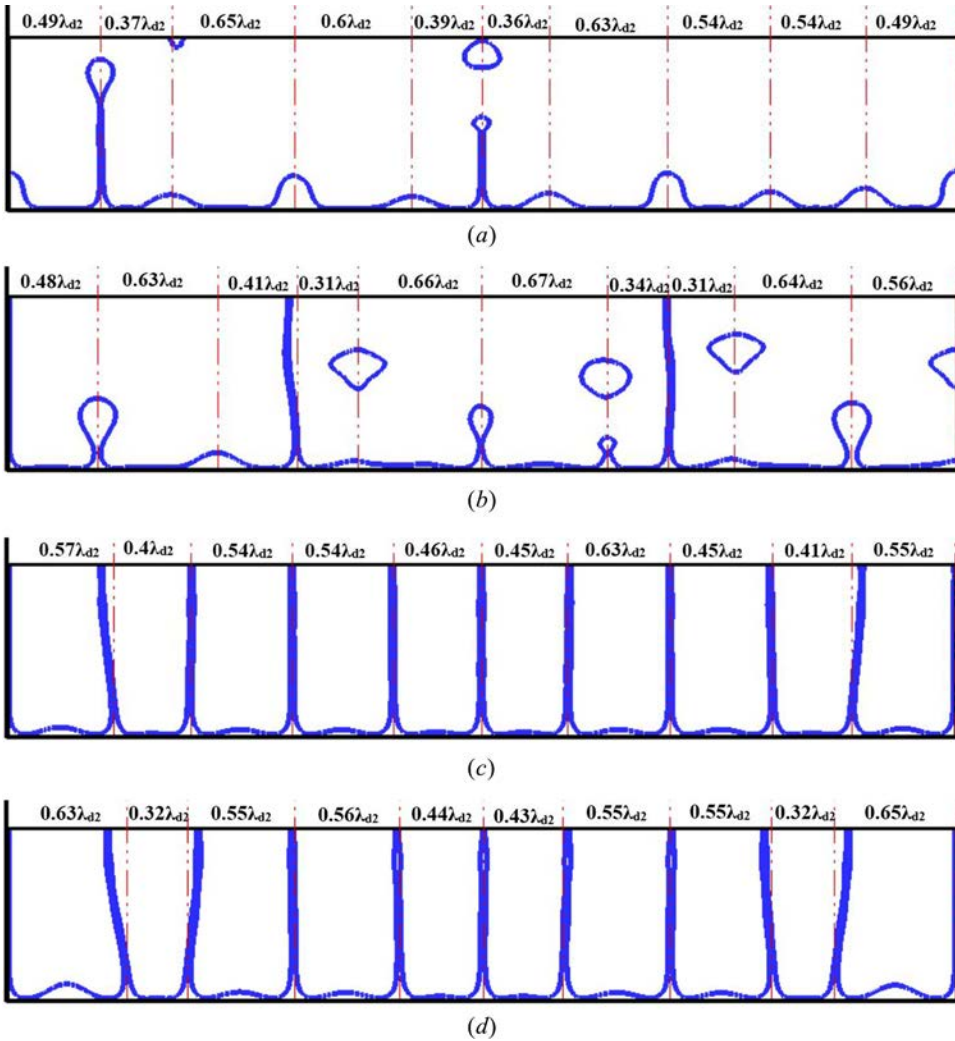


**Figure 9.** Spacing between nodes and antinodes for the near-critical conditions of water at nondimensional time  $\tau = 177.73$  for various Jacob numbers: (a)  $Ja_v = 2.55$ , (b)  $Ja_v = 6.37$ , (c)  $Ja_v = 19.1$ , and (d)  $Ja_v = 25.47$ .

Westwater [5] found from their experimental study of film boiling of water at the atmospheric conditions that the average spacing between two bubble releasing locations is larger than the critical wavelength  $\lambda_c$  and close to  $\lambda_{d2}$ . The present numerical results agree well with the experimental results of [5].

Figures 10a and 10b show the periodic variations of space averaged Nusselt numbers over the superheated wall at low values of  $Ja_v = 2.547$  and 6.367. The transient variation of space averaged Nusselt number obtained from the present numerical study is compared with the values obtained from the correlations of Berenson [3], Klimenko [6], and Son and Dhir [10], and are shown in Figure 10a for  $Ja_v = 2.547$ . The averaged Nusselt number obtained using the multimode film boiling model of the present study agrees well with that of Son and Dhir [10]. The periodic variation of Nusselt number is due to the periodic release of vapor bubbles as shown in Figures 6a and 6b, respectively. Figures 10c and 10d show the space averaged Nusselt number for higher  $Ja_v$  values of 19.103 and 25.47. The space averaged Nusselt number remains almost constant after the first ebullition cycle due to the formation of jets of stable vapor columns as shown in Figures 8a and 8b, respectively.

For  $\tau \geq 150$ , the periodic fluctuation of space and time averaged Nusselt number becomes independent of the initial conditions such as the initial vapor film thickness,  $\delta(x)$ , and the temperature profile initialized within the vapor layer [10]. Hence, in the present numerical study, the time averaged Nusselt numbers are computed for  $\tau \geq 150$  onward. These results show that the time averaged Nusselt number obtained from the single-mode film boiling model overpredicts in comparison with that of the multimode model as shown in Figure 11. The time averaged Nusselt number obtained

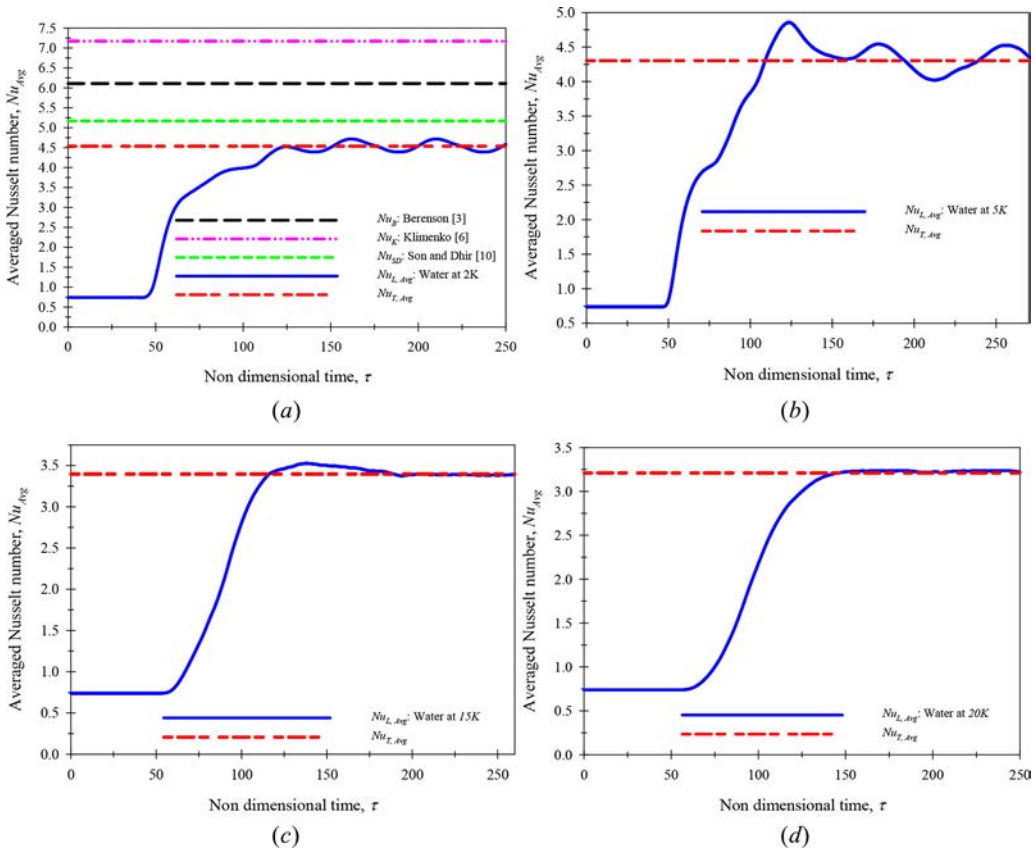


**Figure 10.** Variation of the space and the time averaged Nusselt number obtained using the multimode film boiling model for near-critical conditions of water at different Jacob numbers: (a)  $Ja_v = 2.55$ , (b)  $Ja_v = 6.37$ , (c)  $Ja_v = 19.1$ , and (d)  $Ja_v = 25.47$ .



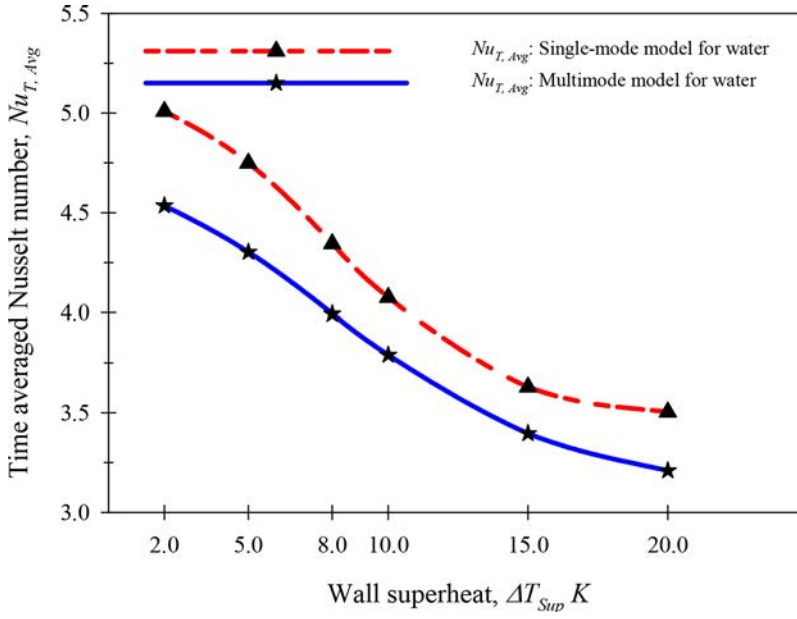


**Figure 11.** Comparison of the time averaged Nusselt number obtained using both the single-mode and the multimode film boiling models for the near-critical conditions of water at different wall superheats,  $\Delta T_{Sup}$ .

from the multimode film boiling model shows the maximum deviation of 9.44% and the minimum deviation of 5.23% with that of the single-mode film boiling model.

## 4.2. Film boiling of R134a

### 4.2.1. Single-mode saturated film boiling model for R134a

The transient evolution of the liquid–vapor interface morphology for refrigerant R134a at various  $Ja_v$  values ranging from 0.163 to 1.63 ( $2 \text{ K} \leq \Delta T_{Sup} \leq 20 \text{ K}$ ) obtained during the first ebullition cycle is shown in Figure 12. Unlike the results obtained for film boiling of water using the single-mode model, the discrete vapor bubble formation is observed for all  $Ja_v$  values considered for R134a. In this study, the maximum  $Ja_v$  corresponding to  $\Delta T_{Sup} = 20 \text{ K}$  is 1.63, which is much less than the lowest  $Ja_v$  of 2.547 (at  $\Delta T_{Sup}$  of 2 K) considered for water. In Figures 3a–3c, for water the formation of the discrete periodic bubble release cycle was observed at nodes and antinodes up to  $Ja_v \leq 10.19$ .

For the case of R134a, at lower  $Ja_v = 0.163$  ( $\Delta T_{Sup} = 2 \text{ K}$ ), the bubble release period of  $\tau = 75$  is less compared with one bubble release cycle of water for which  $\tau$  is around 125. Hence, for the total non-dimensional time duration  $\tau_{max} = 650$ , more number of ebullition cycles occurs for refrigerant R134a as compared to that of water. Because the rate of mass transfer is inversely proportional to the latent heat of vaporization, the latent heat  $h_{lv}$  value of water is higher compared to refrigerant R134a (in Tables 1 and 2). Hence, higher heat and mass transfer rate and lower bubble release period are observed for R134a as compared to that of water. Therefore, the thermo-physical properties of working fluids have a significant effect on the periodic bubble release cycle of saturated film boiling flows. Hence, the thermo-physical properties of working fluid play a significant role in the flow and heat transfer characteristics.

The variation of space averaged Nusselt number with respect to  $\tau$  for various  $Ja_v$  values is shown in Figure 13. This figure shows that the Nusselt number variation is not periodic although discrete bubbles are released. Hence, the bubbles are also not released periodically. Similar variation of the space averaged Nusselt number was also observed by Tomar et al. [18] for R134a at  $\Delta T_{Sup}$  values of 10 K, 30 K, and 50 K. The difference between the averaged Nusselt number obtained from the present numerical simulations and the value obtained from the correlation of Berenson [3] and Klimenko

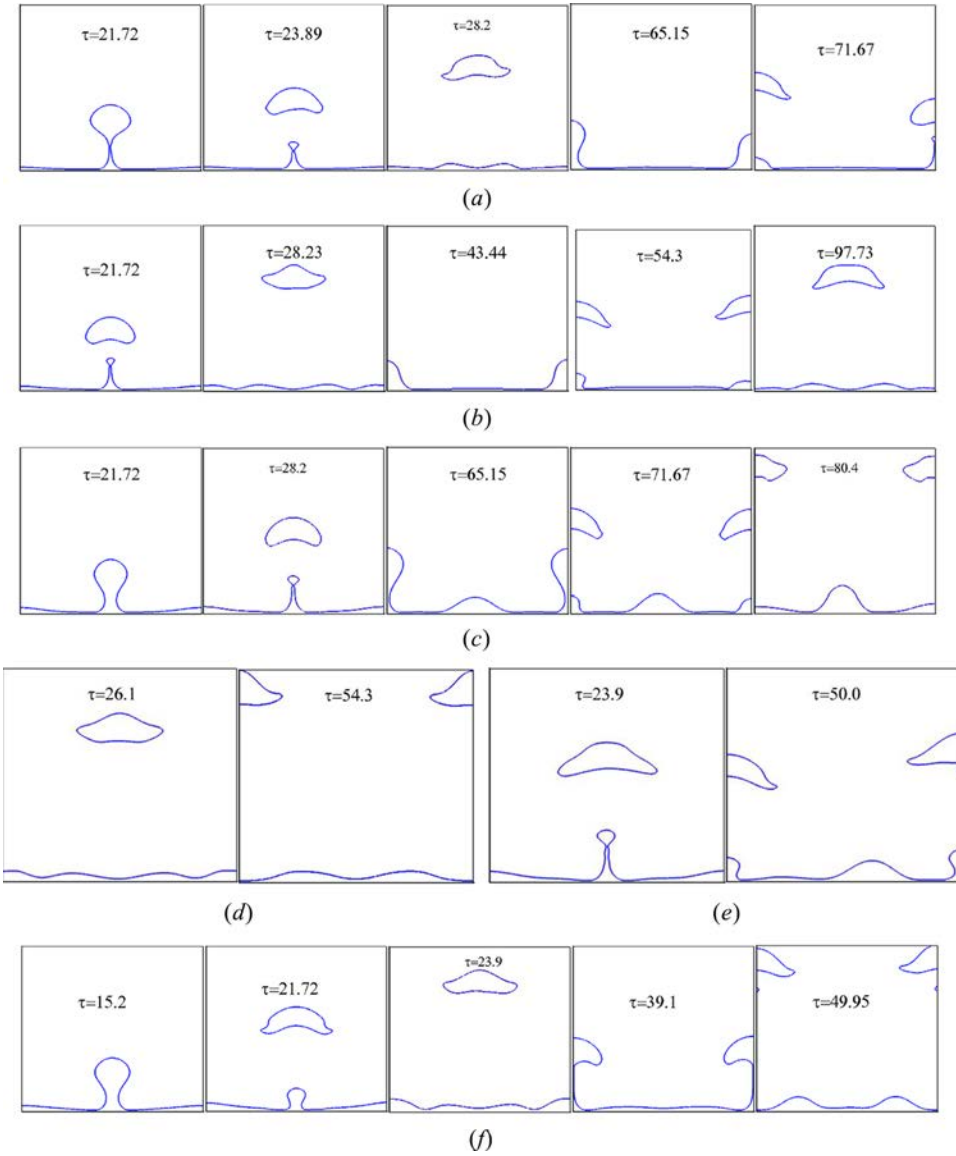


**Figure 12.** Interface morphologies of the periodic bubble release cycle obtained using the single-mode film boiling model for refrigerant R134a at different Jacob numbers: (a)  $J_{a_v} = 0.163$ , (b)  $J_{a_v} = 0.407$ , (c)  $J_{a_v} = 0.651$ , (d)  $J_{a_v} = 0.814$ , (e)  $J_{a_v} = 1.221$ , and (f)  $J_{a_v} = 1.628$ .

[6] is significant for  $J_{a_v} = 0.163$ . However, at  $J_{a_v} = 0.407$ , the difference between the time averaged Nusselt number obtained from the present simulation and the values obtained from the correlation of Berenson [3] is less.

As the single-mode boiling model has its own limitations, in the next section, the results obtained from the multimode boiling model of R134a are presented to understand the flow and heat transfer characteristics better and also to compare the averaged Nusselt number obtained from the single-mode and multimode models.

#### 4.2.2. Multimode saturated film boiling model for R134a

Saturated film boiling over a horizontal flat surface has been simulated using the multimode boiling model at a near-critical condition of refrigerant R134a for  $J_{a_v}$  values,  $0.163 \leq J_{a_v} \leq 1.63$

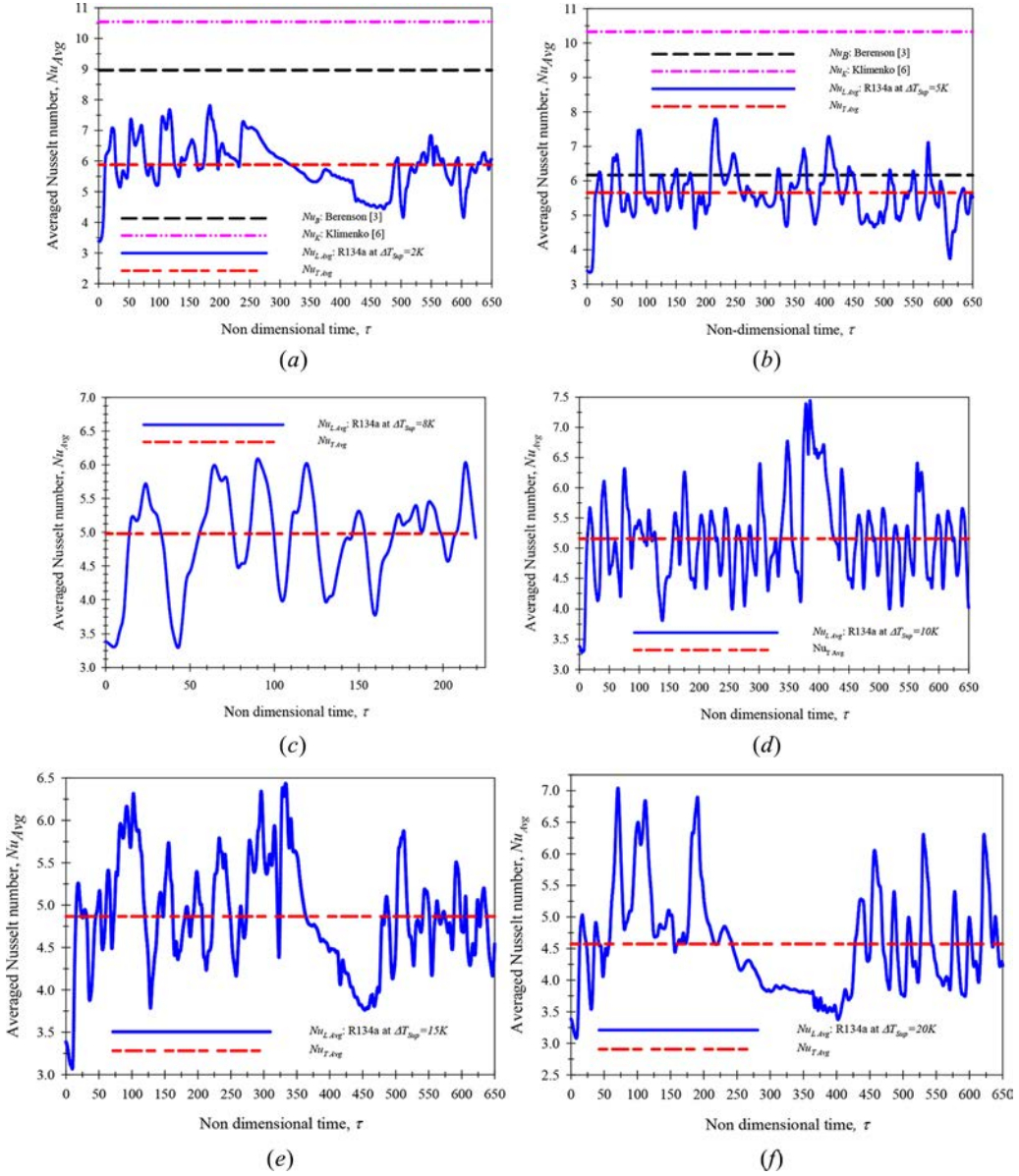


**Figure 13.** Transient variation of the space and the time averaged Nusselt numbers for refrigerant R134a obtained with the single-mode film boiling model at different Jacob numbers (a)  $Ja_v = 0.163$ , (b)  $Ja_v = 0.407$ , (c)  $Ja_v = 0.651$ , (d)  $Ja_v = 0.814$ , (e)  $Ja_v = 1.222$ , and (f)  $Ja_v = 1.629$ .

( $2K \leq \Delta T_{sup} \leq 20K$ ). The computational domain size of  $5\lambda_{d2} \times \lambda_{d2}$  is selected similar to that of film boiling of water. The evolution of the liquid-vapor interface morphology during the bubble release cycle obtained for three different  $Ja_v$  values of 0.163, 0.814, and 1.63 is shown in Figure 14. The corresponding  $\Delta T_{sup}$  values are 2 K, 10 K, and 20 K, respectively. All the results presented here are from  $\tau \geq 184.6$  to show the results of the established periodic ebullition cycle. For all  $Ja_v$  values, within the computational domain width of  $5\lambda_{d2}$ , at least one vapor column forms and bubbles are released at the end of the vapor column periodically. After a few bubbles are released, the vapor column collapses. The length of the vapor column increases as  $Ja_v$  increases. Hence, the stability of the vapor column is dependent on the magnitude of  $Ja_v$ .



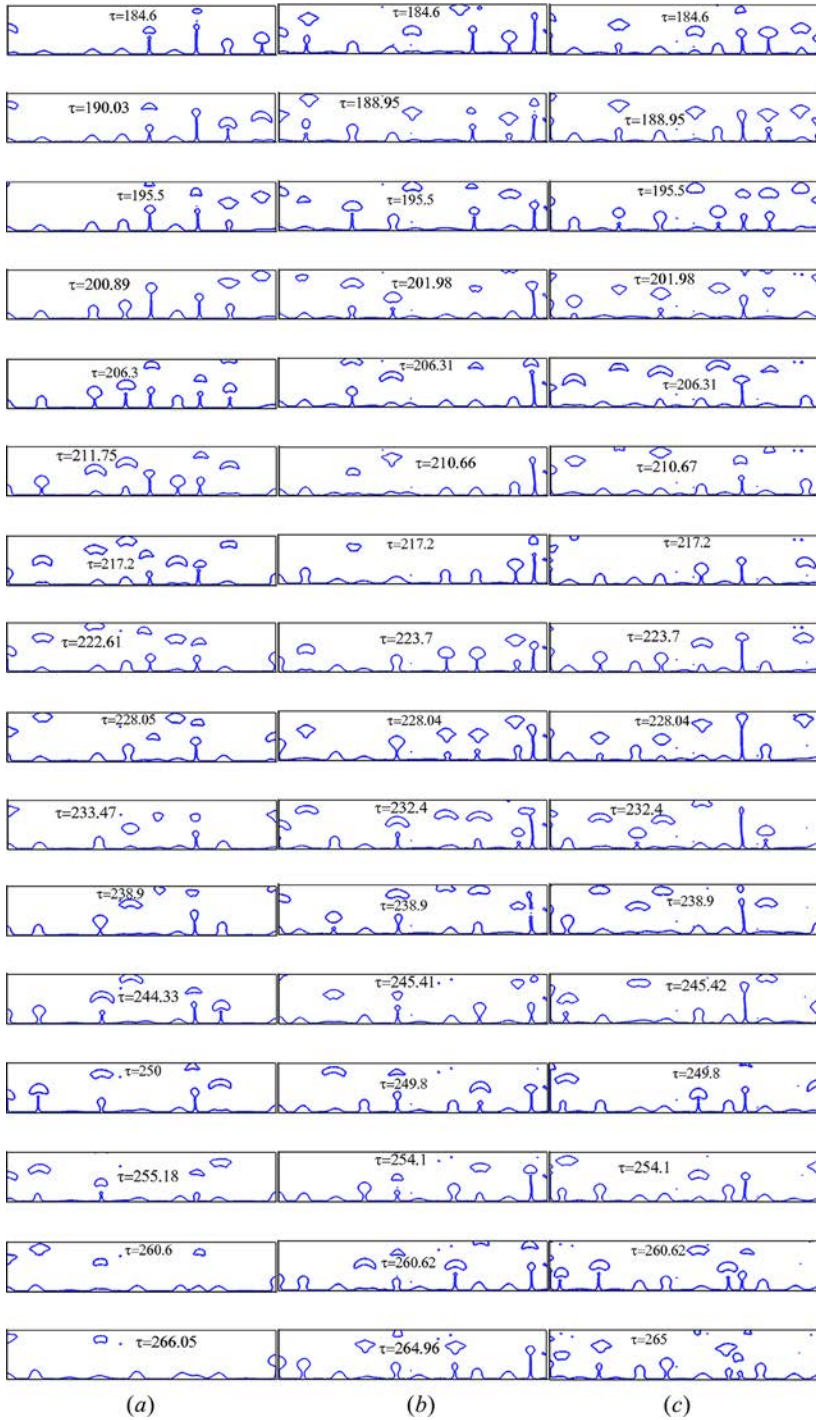


**Figure 14.** Evolution of the interface morphology obtained with the multimode film boiling model for refrigerant R134a at Jacob numbers: (a)  $Ja_v = 0.163$  ( $\Delta T_{sup} = 2$  K), (b)  $Ja_v = 0.814$  ( $\Delta T_{sup} = 10$  K), and (c)  $Ja_v = 1.628$  ( $\Delta T_{sup} = 20$  K).

Figure 15 shows the periodic evolution of the interface morphology for R134a with the corresponding spatial variations of the local Nusselt number distribution. The vapor layer is thicker in the region where the bubble grows and about to depart from the vapor layer. Thin vapor layer forms

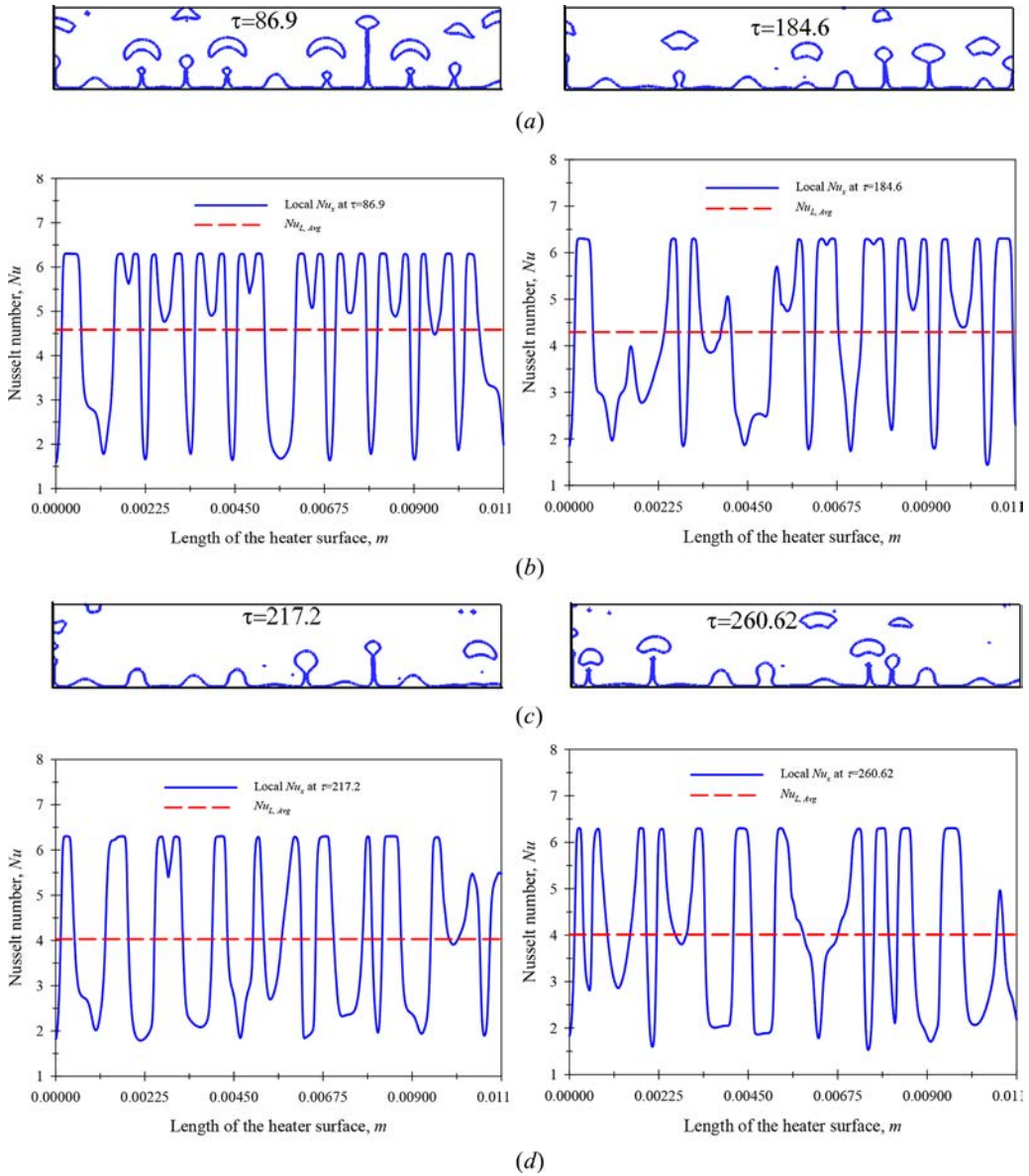


**Figure 15.** Interface evolution obtained from the multimode film boiling model and the corresponding variation of a local Nusselt number for R134a at Jacob number  $Ja_v = 1.63$ : (a) interface morphology obtained at  $\tau = 86.9$  and  $\tau = 184.6$ , (b) the variation of local Nusselt number obtained at  $\tau = 86.9$  and  $\tau = 184.6$ , (c) interface morphology obtained at  $\tau = 217.2$  and  $\tau = 260.62$ , and (d) the variation of local Nusselt number obtained at  $\tau = 217.2$  and  $\tau = 260.62$ .

when the vapor layer withdraws toward the hot plate after releasing a vapor bubble. These results show that the magnitude of the local Nusselt number is higher at the thin region of the vapor films and is lower at the thick region of the vapor films.

The spacing between nodes and antinodes varies randomly over the heated surface during the periodic bubble release for all  $Ja_v$  values. The distances between the nodes and the antinodes based on  $\lambda_{d2}$  at various  $Ja_v$  values are shown in Figure 16. The smallest and the largest distance between the nodes are  $0.64\lambda_{d2}$  and  $1.48\lambda_{d2}$ , respectively. These values are in close agreement with the results of Esmaeeli and Tryggvason [17], who investigated film boiling of water with the two-dimensional multimode boiling model. The present numerical study shows that the average spacing between the nodes is

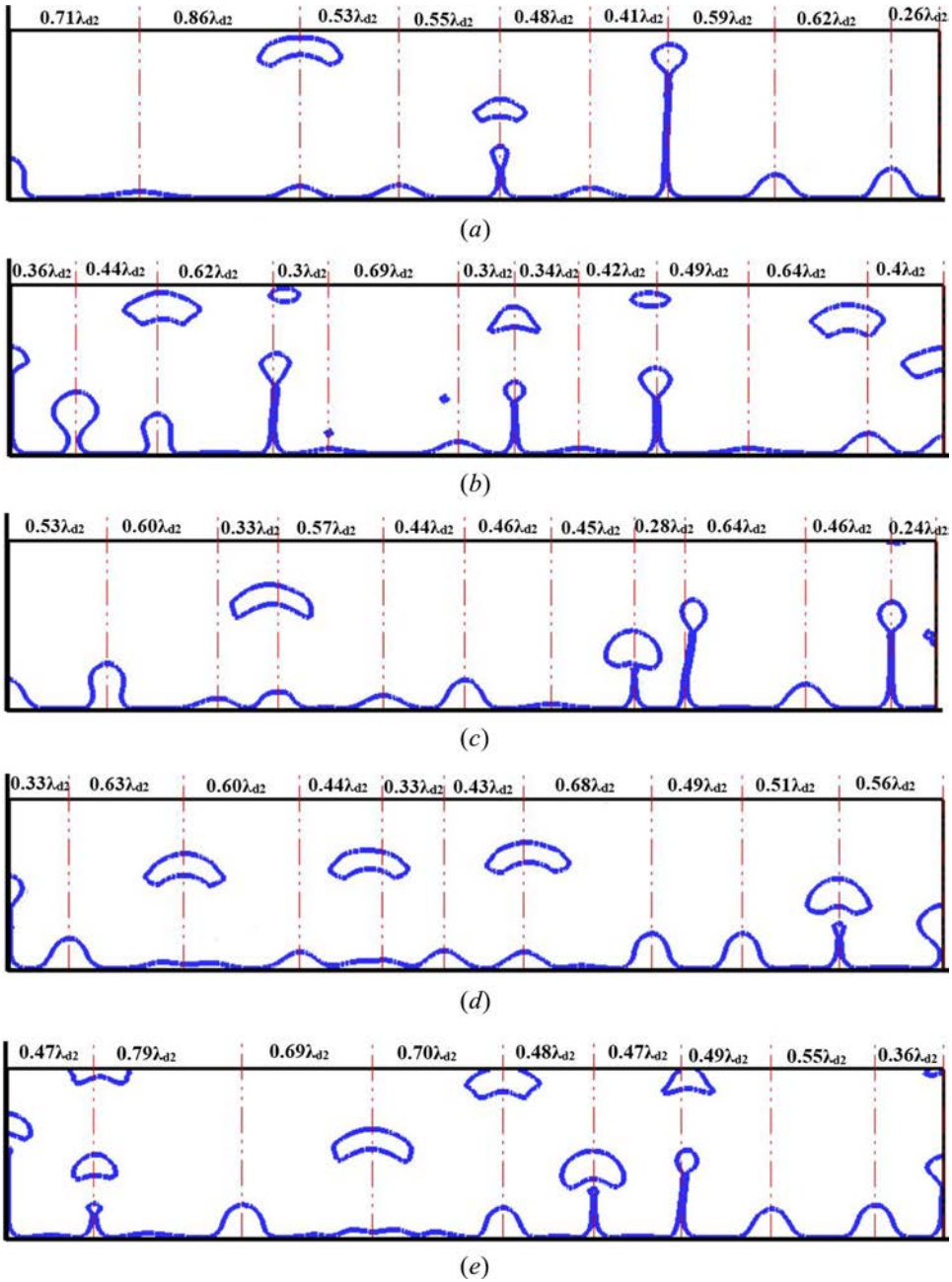


**Figure 16.** Spacing between nodes and antinodes for the near-critical conditions of refrigerant R134a at nondimensional time  $\tau = 168.32$  for various Jacob numbers: (a)  $Ja_v = 0.163$ , (b)  $Ja_v = 0.407$ , (c)  $Ja_v = 0.814$ , (d)  $Ja_v = 1.222$ , and (e)  $Ja_v = 1.629$ .

larger than the critical wavelength and close to  $\lambda_{d2}$  as observed by Hosler and Westwater [5], similar to that of water.

Based on the temperature distribution obtained from the present numerical simulations, the space averaged Nusselt numbers were calculated at  $\tau = 5.39$ . Figure 17 shows the variations of the space averaged Nusselt numbers obtained at different  $Ja_v$  values. From these results it is observed that as  $Ja_v$  increases, the magnitude of the time averaged Nusselt number decreases. After the first ebullition cycle, the periodic variation of the space averaged Nusselt number becomes almost independent of the

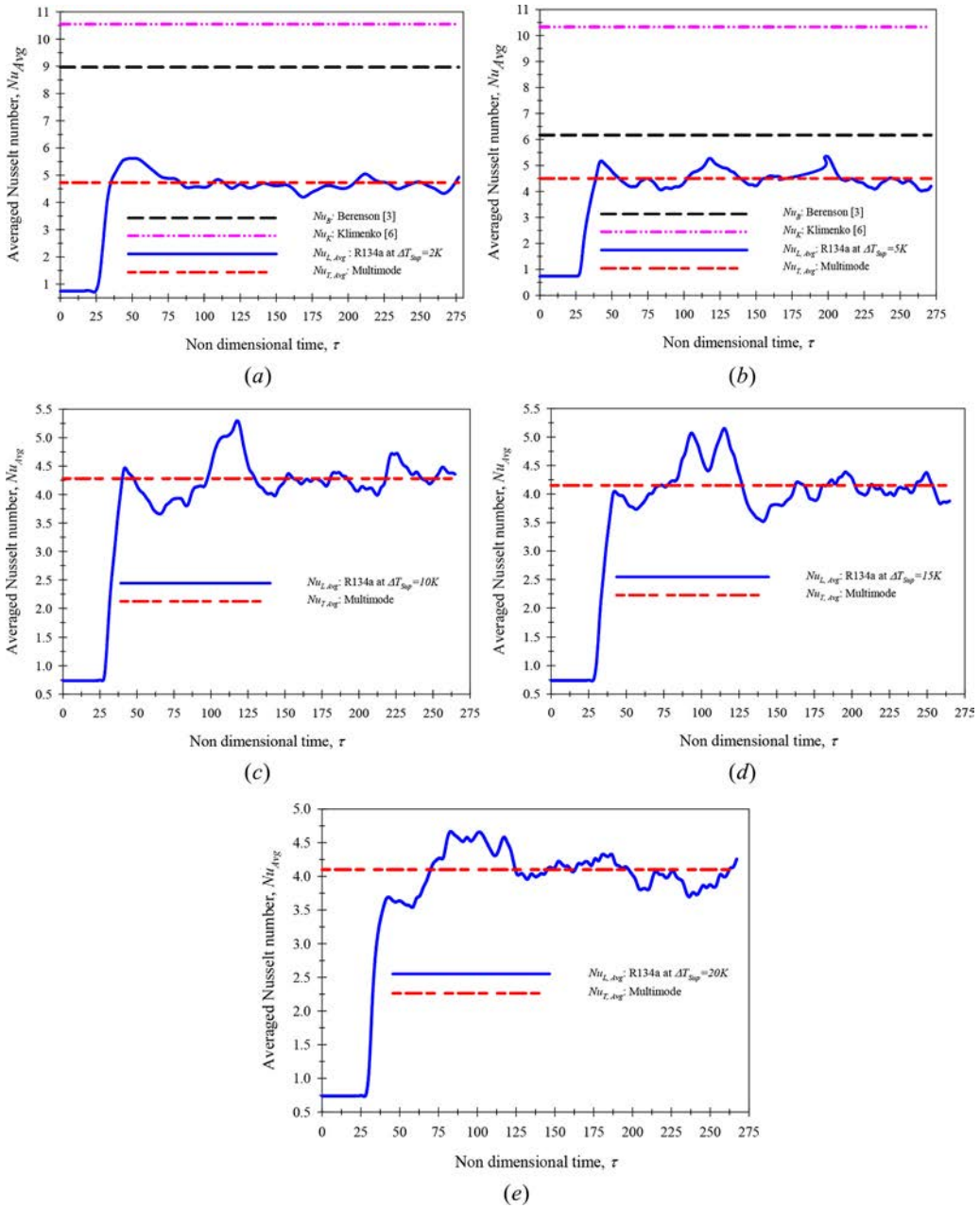


**Figure 17.** The variation of the space and the time averaged Nusselt numbers obtained using the multimode film boiling model for the near-critical conditions of R134a at different Jacob numbers: (a)  $Ja_v = 0.163$ , (b)  $Ja_v = 0.407$ , (c)  $Ja_v = 0.814$ , (d)  $Ja_v = 1.222$ , and (e)  $Ja_v = 1.629$ .

initial conditions [10]. In Figure 17a, the average Nusselt number values obtained for  $Ja_v = 0.163$  and the values obtained from the Berenson [3] and Klimenko [6] correlations are shown. The averaged Nusselt number predicted from the present numerical simulation underpredicts significantly compared to that of the above-mentioned correlations. However, at  $Ja_v = 0.407$ , the deviation between the Nusselt number obtained from the present numerical study and that of Berenson is around 27%.

In Figure 18, the time averaged Nusselt numbers obtained from the single-mode and multimode film boiling models obtained for R134a are compared. As observed in the case of film boiling of water,



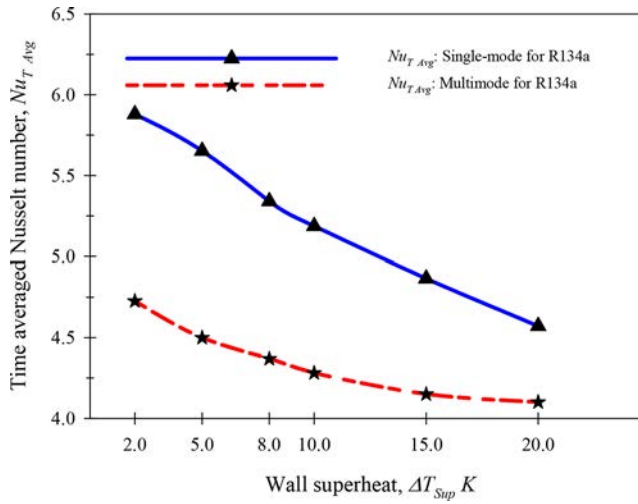


**Figure 18.** Comparison of the time averaged Nusselt number obtained using both the single-mode and the multimode film boiling models for the near-critical conditions of refrigerant R134a at different wall superheats,  $\Delta T_{Sup}$ .

the single-mode film boiling model overpredicts the time averaged Nusselt number as compared to the multimode film boiling model. The time averaged Nusselt number obtained from the multimode film boiling model shows the maximum deviation of 19.78% and the minimum deviation of 10.74% with that of the single-mode film boiling model.

## 5. Conclusions

In this numerical study, natural convection saturated film boiling over a flat horizontal surface was investigated using both single-mode and multimode film boiling models using a multidirectional advection algorithm of the CLSVOF interface capturing method. In this study, water and R134a were considered as working fluids. For both working fluids, near-critical conditions were considered for film boiling studies. Simulations were carried out for a wide range of  $Ja_v$ . Based on the present study, the following conclusions are arrived at.

1. In the case of water, the single-mode film boiling model predicts discrete bubble formations at nodes and antinodes alternatively up to  $Ja_v \leq 10.19$ . For  $Ja_v$  values of 12.74 and 19.1, the formation of stable vapor columns is observed. However, at the higher  $Ja_v$  of 25.47, the vapor columns are unstable.
2. Even at low  $Ja_v$  of 2.55, the results obtained from the multimode film boiling model of water show two stable vapor columns (within the domain width of  $5\lambda_{d2}$ ), which release bubbles at the tip of the vapor column periodically. At the other locations, discrete bubbles are released at nodes and antinodes. At  $Ja_v$  of 19.1, stable vapor columns are observed. However, the columns become unstable at  $Ja_v$  of 25.47.
3. In the case of R134a, the single-mode model predicts discrete bubble release at both nodes and antinodes alternatively for the range of  $Ja_v$  values considered. In the case of the multimode model, discrete bubbles are released at both nodes and antinodes alternatively excluding one location where bubbles release at the tip of a vapor column, which may or may not be stable.
4. The average spacing between the nodes varies from critical wavelength  $\lambda_c$  to  $\lambda_{d2}$  for all  $Ja_v$  considered for both water and R134a.
5. For both water and R134a, the magnitude of time averaged Nusselt number obtained from the single-mode film boiling model shows overprediction compared to that of the multimode boiling model. For both fluids, as  $Ja_v$  increases, the time averaged Nusselt number decreases.

## Acknowledgments

The authors acknowledge the high-performance computing facility provided by the Computer Service Center at IIT Delhi.

## Funding

This research work was carried out under the research Grant, No. SR/S3/MERC-0118/2009, sponsored by the Department of Science and Technology (DST), India.

## References

- [1] Y. P. Chang, A Theoretical Analysis of Heat Transfer in Natural Convection and in Boiling, *J. Heat Transfer*, vol. 79, pp. 1501–1509, 1957.
- [2] Y. P. Chang, Wave Theory of Heat Transfer in Film Boiling, *J. Heat Transfer*, vol. 81, pp. 1–12, 1959.
- [3] P. J. Berenson, Film Boiling Heat Transfer from a Horizontal Surface, *J. Heat Transfer*, vol. 83, pp. 351–356, 1961.
- [4] V. M. Borishansky Heat Transfer to a Liquid Freely Flowing Over a Surface Heated to a Temperature Above the Boiling Point, in Problems of Heat Transfer During a Change of State by S. S. Kutateladze, AEC-tr-3405, 1959.
- [5] E. R. Hosler and J. W. Westwater, Film Boiling on a Horizontal Plate, *ARS J.*, vol. 32, pp. 553–558, 1962.
- [6] V. V. Klimenko, Film Boiling on a Horizontal Plate- New Correlation, *Int. J. Heat Mass Transfer*, vol. 24, pp. 69–79, 1981.
- [7] V. V. Klimenko and A. G. Shelepen, Film Boiling on a Horizontal Plate- A Supplementary Communication, *Int. J. Heat Mass Transfer*, vol. 25, pp. 1611–1613, 1982.
- [8] M. R. Duijn, G. A. Greene, and T. F. Irvine Jr, Measurement of Film Boiling Bubble Parameters on a Horizontal Plate, *Int. Comm. Heat Mass Transfer*, vol. 16, pp. 355–366, 1989.
- [9] G. Son and V. K. Dhir, Numerical Simulation of Saturated Film Boiling on a Horizontal Surface, *J. Heat Transfer*, vol. 119, pp. 525–533, 1997.
- [10] G. Son and V. K. Dhir, Numerical Simulation of Film Boiling Near Critical Pressures with a Level Set Method, *J. Heat Transfer*, vol. 120, pp. 183–192, 1998.
- [11] D. Juric and G. Tryggvason, Computation of Boiling Flows, *Int. J. Multiphase Flow*, vol. 24, pp. 387–410, 1998.
- [12] S. W. J. Welch and J. Wilson, A Volume of Fluid Based Method for Fluid Flows with Phase Change, *J. Comput. Phys.*, vol. 160, pp. 662–682, 2000.
- [13] S. W. J. Welch and T. Rachidi, Numerical Computation of Film Boiling Including Conjugate Heat Transfer, *Numer. Heat Transfer, Part B Fundam.*, vol. 42, pp. 35–53, 2002.
- [14] S. Shin and D. Juric, Modeling Three-Dimensional Multiphase Flow Using a Level Contour Reconstruction Method for Front Tracking Without Connectivity, *J. Comput. Phys.*, vol. 180, pp. 427–470, 2002.
- [15] D. K. Agarwal, S. W. J. Welch, G. Biswas, and F. Durst, Planar Simulation of Bubble Growth in Film Boiling in Near-Critical Water Using a Variant of the VOF Method, *J. Heat Transfer*, vol. 126, pp. 329–338, 2004.
- [16] A. Esmarelli and G. Tryggvason, Computation of Film Boiling Part I: Numerical Method, *Int. J. Heat Mass Transfer*, vol. 47, pp. 5451–5461, 2004.
- [17] A. Esmarelli and G. Tryggvason, Computation of Film Boiling Part II: Multi-Mode Film Boiling, *Int. J. Heat Mass Transfer*, vol. 47, pp. 5463–5476, 2004.
- [18] G. Tomar, G. Biswas, A. Sharma, and A. Agrawal, Numerical Simulation of Bubble Growth in Film Boiling Using CLSVOF Method, *Phys. Fluids*, vol. 17, pp. (112103) 1–13, 2005.
- [19] G. Tomar, G. Biswas, A. Sharma, and S. W. J. Welch, Multimode Analysis of Bubble Growth in Saturated Film Boiling, *Phys. Fluids*, vol. 20, pp. (092101) 1–7, 2008.
- [20] A. Hens, G. Biswas, and S. De, Analysis of Interfacial Instability and Multimode Bubble Formation in Saturated Boiling Flows Using Coupled Level Set and Volume of Fluid Approach, *Phys. Fluids*, vol. 26 pp. (012105) 1–14, 2014.
- [21] F. Gibou, L. Chen, D. Nguyen, and S. Banerjee, A Level Set Based Sharp Interface Method for the Multiphase Incompressible Navier-Stokes Equations with Phase Change, *J. Comput. Phys.*, vol. 222, pp. 536–555, 2007.
- [22] V. H. Gada and A. Sharma, on a Novel Dual-Grid Level-Set Method for Two-Phase Flow Simulation, *Numer. Heat Transfer Part B Fundam.*, vol. 59, pp. 26–57, 2011.
- [23] D. Z. Guo, D. L. Sun, Z. Y. Li, and W. Q. Tao, Phase Change Heat Transfer Simulation for Boiling Bubbles Arising from a Vapor Film by the VOSET Method, *Numer. Heat Transfer Part A Appl.*, vol. 59, pp. 857–881, 2011.
- [24] B. M. Ningegowda and B. Premachandran, A Coupled Level Set and Volume of Fluid Method with Multi-Directional Advection Algorithms for Two-Phase with and Without Phase Change, *Int. J. Heat Mass Transfer*, vol. 79, pp. 532–550, 2014.
- [25] Y. Tsui, S. Lin, Y. Lai, and F. Wu, Phase Change Calculations for Film Boiling Flows, *Int. J. Heat Mass Transfer*, vol. 70, pp. 745–757, 2014.

- [26] J. U. Brackbill, D. B. Kothe, and C. Zemach, A Continuum Method for Modeling Surface Tension, *J. Comput. Phys.*, vol. 100, pp. 335–354, 1992.
- [27] M. Sussman and E. G. Puckett, A Coupled Level Set and Volume of Fluid Method for Computing 3D and Axisymmetric Incompressible Two-Phase Flows, *J. Comput. Phys.*, vol. 162, pp. 301–337, 2000.
- [28] G. Son and N. Hur, A Coupled Level-Set and Volume-of-Fluid Method for the Buoyancy-Driven Motion of Fluid Particles, *Numer. Heat Transfer Part B Fundam.*, vol. 42, pp. 523–542, 2002.
- [29] J. Lopez, J. Hernandez, P. Gomez, and F. Faura, A Volume of Fluid Method Based on Multidimensional Advection and Spline Interface Reconstruction, *J. Comput. Phys.*, vol. 195, pp. 718–742, 2004.
- [30] J. Lopez and J. Hernandez, Analytical and geometrical tools for 3D Volume of Fluid Methods in General Grids, *J. Comput. Phys.*, vol. 227, pp. 5939–5948, 2008.
- [31] D. L. Youngs Time-Dependent Multi-Material Flow with Large Fluid Distortion, in W. Morton M. J. Baines (eds.), *Numerical Methods for Fluid Dynamics*, Academic Press, New York, pp. 273–285, 1982.
- [32] W. J. Rider and D. B. Kothe, Reconstructing Volume Tracking Methods, *J. Comput. Phys.*, vol. 141, pp. 112–152, 1998.
- [33] S. Osher and J. A. Sethian, Fronts Propagating with Curvature-Dependent Speed: Algorithm Based on Hamilton–Jacobi Formulations, *J. Comput. Phys.*, vol. 79, pp. 12–49, 1988.
- [34] T. Hayase, J. A. C. Humphrey, and R. Greif, A Consistently Formulated QUICK Scheme for Fast and Stable Convergence Using Finite-Volume Iterative Calculation Procedures, *J. Comput. Phys.*, vol. 98, pp. 108–118, 1992.
- [35] M. Reimann and U. Grigull, Wärmeübergangbeifreier Konvektion und FilmsiedenimkritischenGebiet von Wasser und Kohlendioxid, *Warme-und Stof-Fubertragung*, vol. 81, pp. 229–239, 1975.
- [36] E. Abadzic and R. J. Goldstein, Film Boiling and Free Convection Heat Transfer to Carbon Dioxide Near the Critical State, *Int. J. Heat Mass Transfer*, vol. 13, pp. 1163–1175, 1970.